J|A|C|S
ARTICLES
Published on Web 03/01/2002

Organometallic Ruthenium(II) Diamine Anticancer Complexes: Arene-Nucleobase Stacking and Stereospecific Hydrogen-Bonding in Guanine Adducts

Haimei Chen, John A. Parkinson, Simon Parsons, Robert A. Coxall, Robert O. Gould, and Peter J. Sadler*

Contribution from the Department of Chemistry, University of Edinburgh, West Mains Road, Edinburgh EH9 3JJ, U.K.

Received November 7, 2001

Abstract: Organometallic ruthenium(II) arene anticancer complexes of the type [(η^6-arene)Ru(II)(en)Cl][PF_6] (en = ethylenediamine) specifically target guanine bases of DNA oligomers and form monofunctional adducts (Morris, R., et al. *J. Med. Chem.* **2001**). We have determined the structures of monofunctional adducts of the "piano-stool" complexes [(η^6-Bip)Ru(II)(en)Cl][PF_6] (**1**, Bip = biphenyl), [(η^6-THA)Ru(II)(en)Cl][PF_6] (**2**, THA = 5,8,9,10-tetrahydroanthracene), and [(η^6-DHA)Ru(II)(en)Cl][PF_6] (**3**, DHA = 9,10-dihydroanthracene) with guanine derivatives, in the solid state by X-ray crystallography, and in solution using 2D [^{1}H,^{1}H] NOESY and [^{1}H,^{15}N] HSQC NMR methods. Strong $\pi-\pi$ arene-nucleobase stacking is present in the crystal structures of [(η^6-$C_{14}H_{14}$)Ru(en)(9EtG-*N7*)][PF_6]$_2$·(MeOH) (**6**) and [(η^6-$C_{14}H_{12}$)Ru(en)(9EtG-*N7*)][PF_6]$_2$·2(MeOH) (**7**) (9EtG = 9-ethylguanine). The anthracene outer ring (C) stacks over the purine base at distances of 3.45 Å for **6** and 3.31 Å for **7**, with dihedral angles of 3.3° and 3.1°, respectively. In the crystal structure of [(η^6-biphenyl)Ru(en)(9EtG-*N7*)][PF_6]$_2$·(MeOH) (**4**), there is intermolecular stacking between the pendant phenyl ring and the purine six-membered ring at a distance of 4.0 Å (dihedral angle 4.5°). This stacking stabilizes a cyclic tetramer structure in the unit cell. The guanosine (Guo) adduct [(η^6-biphenyl)Ru(en)(Guo-*N7*)][PF_6]$_2$·3.75(H_2O) (**5**) exhibits intramolecular stacking of the pendant phenyl ring with the purine five-membered ring (3.8 Å, 23.8°) and intermolecular stacking of the purine six-membered ring with an adjacent pendant phenyl ring (4.2 Å, 23.0°). These occur alternately giving a columnar-type structure. A syn orientation of arene and purine is present in the crystal structures **5**, **6**, and **7**, while the orientation is anti for **4**. However, in solution, a syn orientation predominates for all the biphenyl adducts **4**, **5**, and the guanosine 5′-monophosphate (5′-GMP) adduct **8** [(η^6-biphenyl)Ru(II)(en)(5′-GMP-*N7*)], as revealed by NMR NOE studies. The predominance of the syn orientation both in the solid state and in solution can be attributed to hydrophobic interactions between the arene and purine rings. There are significant reorientations and conformational changes of the arene ligands in [(η^6-arene)Ru(II)(en)(G-*N7*)] complexes in the solid state, with respect to those of the parent chloro-complexes [(η^6-arene)Ru(II)(en)Cl]$^+$. The arene ligands have flexibility through rotation around the arene-Ru π-bonds, propeller twisting for Bip, and hinge-bending for THA and DHA. Thus propeller twisting of Bip decreases by ca. 10° so as to maximize intra- or intermolecular stacking with the purine ring, and stacking of THA and DHA with the purine is optimized when their tricyclic ring systems are bent by ca. 30°, which involves increased bending of THA and a flattening of DHA. This flexibility makes simultaneous arene-base stacking and N7-covalent binding compatible. Strong stereospecific intramolecular H-bonding between an en NH proton oriented away from the arene (en NH(d)) and the C6 carbonyl of G (G O6) is present in the crystal structures of **4**, **5**, **6**, and **7** (average N···O distance 2.8 Å, N−H···O angle 163°). NMR studies of the 5′-GMP adduct **8** provided evidence that en NH(d) protons are involved in strong H-bonding with the 5′-phosphate and O6 of 5′-GMP. The strong H-bonding from G O6 to en NH(d) protons partly accounts for the high preference for binding of {(η^6-arene)Ru(II)en}$^{2+}$ to G versus A (adenine). These studies suggest that simultaneous covalent coordination, intercalation, and stereospecific H-bonding can be incorporated into Ru(II) arene complexes to optimize their DNA recognition behavior, and as potential drug design features.

Introduction

Ruthenium complexes offer potential for the design of anticancer drugs.[1] The ammine complex *fac*-[Ru(III)$Cl_3(NH_3)_3$] has long been known to be active, but its poor aqueous solubility has prevented its clinical use.[2] Recently other Ru complexes such as *trans*-[Ru(II)Cl_2(DMSO)$_4$], *trans*-[HIn][Ru(III)Cl_4(Ind)$_2$] (Ind = indazole), *mer*-[Ru(III)(terpy)Cl_3] (terpy = 2,2′:6′,2″-terpyridine), α-[Ru(azpy)$_2Cl_2$] (azpy = 2-(phenylazo)pyridine),

(1) Clarke, M. J.; Zhu, F.; Frasca, D. R. *Chem. Rev.* **1999**, *99*, 2511−2533.

(2) Clarke, M. J. *Met. Ions Biol. Syst.* **1980**, *11*, 231−283.

10.1021/ja017482e CCC: $22.00

and [Ru(IV)(cdta)Cl_2] (cdta = 1,2-cyclohexanediaminetetraacetate) have also been reported to be highly active.[3] *trans*-[HIm][Ru(III)Cl_4(DMSO)(Im)] (Im = imidazole) (NAMI-A) recently became the first Ru complex to enter clinical trials. NAMI-A is relatively nontoxic, but active against tumor metastases.[4] Ru(III) antitumor complexes may serve as prodrugs which are reduced to active Ru(II) species in vivo.[5] We have found that organometallic Ru(II) complexes of the type [(η^6-arene)Ru(II)(en)Cl][PF_6] (en = ethylenediamine) exhibit anticancer activity both in vitro[6,7] and in vivo,[8] including activity against cisplatin-resistant cancer cells.

A potential target for these organometallic Ru(II) complexes is DNA, and in initial studies we observed strong selective binding to N7 of guanine (G) bases on DNA oligomers.[7] It is now important to elucidate potential modes of interaction of these Ru arene complexes with DNA and, in particular, to investigate whether monofunctional binding induces significant structural changes in DNA. Such understanding will be aided by investigations of interactions with mononucleobase derivatives. However, to date only one X-ray crystal structure of a Ru arene adduct with a G derivative, that of [(η^6-C_6H_6)Ru(II)(9EtG-*N7*)$_2$(H_2O)][CF_3SO_3]$_2$·2H_2O, appears to have been reported.[9] Also there are very few reported X-ray crystallographic studies of other Ru(II) and Ru(III)-nucleobase, -nucleoside, or -nucleotide complexes.

Hydrophobic interactions between the arene ligand in [(η^6-arene)Ru(II)(en)Cl]$^+$ and DNA could produce a driving force for DNA binding.[10] Such interactions have already been shown to be of importance in the biological activity of some platinum anticancer agents. Planar aromatic ligands such as doxorubicin,[11] acridine orange,[12] 9-aminoacridine,[13] and ethidium bromide[14] have been incorporated into Pt complexes as potential intercalators. Also, earlier studies of the binding of [Pt(terpy)Cl]$^+$ to calf thymus DNA revealed intercalation as well as covalent interactions.[15] The high antitumor activity of *trans*-[$PtCl_2$(NH_3)L] (L = planar aromatic N donor such as pyridine, thiazole, or quinoline) in comparison with transplatin, *trans*-[$PtCl_2$(NH_3)$_2$],[16,17] has been attributed to the interaction of the quinoline ligand with DNA duplex, perhaps partially by intercalation,[18,19] and the cytotoxic transplatin derivative *trans*-[PtCl(PyAc-*N*,*O*)(NH_3)] (PyAc = pyridin-2-yl-acetate) also appears to exhibit "pseudobifunctional" behavior (covalent/intercalative binding).[20] Hydrophobic interactions with nucleobases play a key role in determining the recognition of cisplatin-modified DNA by the high-mobility group protein (HMG1)[21] and also contribute to formation of stereoselective GG intrastand cross-links on DNA by the anticancer drug *cis*-[$PtCl_2$(NH_3)(2-picoline)].[22] The presence of intercalator ligands in coordinatively saturated octahedral Ru(II), Os(II), and Rh(III) complexes increases DNA affinity and gives rise to highly specific recognition of DNA base sequences via shape selection.[23] Also, the introduction of aliphatic amine ancillary ligands into Rh(III)(phi) complexes (phi = 9,10-phenanthrenequinone diimine) has optimized site-recognition through specific H-bonding and van der Waals contacts between the ancillary ligands and DNA bases.[24] Hydrogen-bonding plays an important role in modulating the DNA sequence recognition of platinum am(m)ine complexes and stabilization of platinated adducts.[25] Pt-am(m)ine NH protons are often involved in H-bonding with an oxygen of the 5′-phosphodiester linkage or with G O6.[26] The diamine ligand in [(η^6-arene)Ru(II)(en)Cl]$^+$ complexes has potential for H-bonding interactions.

The aim of our current work is to gain insight into the factors which influence the interaction of [(η^6-arene)Ru(II)(en)]$^{2+}$ with guanine derivatives, including covalent Ru binding to N7, hydrophobic interactions of the arene ligand, and en NH hydrogen bonding. We have studied the molecular structures of the parent chloro anticancer complexes [(η^6-arene)Ru(en)Cl][PF_6], where arene = biphenyl (Bip, complex **1**), 5,8,9,10-tetrahydroanthracene (THA, **2**), and 9,10-dihydroanthracene (DHA, **3**), and those of their 9-ethylguanine (9EtG), guanosine (Guo), and guanosine 5′-monophosphate (5′-GMP) adducts (Chart 1), where possible both in the solid state by X-ray crystallography and in solution using NMR methods (Table 1). These studies will aid optimization of the design of this new class of anticancer agents.

Experimental Section

Materials. 9-Ethylguanine (Sigma), guanosine hydrate (9-[β-D-ribofuranosyl]guanine) (Aldrich), and Na_2-5′-GMP (Aldrich) were used

(3) (a) Alessio, E.; Mestroni, G.; Nardin, G.; Attia, W. M.; Calligaris, M.; Sava, G.; Zorzet, S. *Inorg. Chem.* **1988**, *27*, 4099−4106. (b) Keppler, B. K.; Henn, M.; Juhl, U. M.; Berger, M. R.; Niebl, R.; Wagner, F. E. *Prog. Clin. Biochem. Med.* **1989**, *10*, 41−69. (c) Nováková, O.; Kaspárková, J.; Vrána, O.; Van Vliet, P. M.; Reedijk, J.; Brabec, V. *Biochemistry* **1995**, *34*, 12369−12378. (d) Velders, A. H.; Kooijman, H.; Spek, A. L.; Haasnoot, J. G.; Vos, D. D.; Reedijk, J. *Inorg. Chem.* **2000**, *39*, 2966−2967. (e) Vilaplana, R. A.; Gonzalez-Vilchez, F.; Gutierrez-Puebla, E.; Ruiz-Valero, C. *Inorg. Chim. Acta* **1994**, *224*, 15−18.

(4) Sava, G.; Gagliardi, R.; Bergamo, A.; Alessio, E.; Mestroni, G. *Anticancer Res.* **1999**, *19*, 969−972.

(5) Clark, M. J.; In *Metal Complexes in Cancer Chemotherapy*; Keppler, B. K., Ed.; VCH: Weinheim, 1993; pp 129−156.

(6) Cummings, J.; Aird, R. E.; Morris, R. E.; Chen, H.; Murdoch, P. del S.; Sadler, P. J.; Smyth, J. F.; Jodrell, D. I. *Clin. Cancer Res.* **2000**, *6* (suppl. S Nov), 142.

(7) Morris, R. E.; Aird, R. E.; Murdoch, P. del S.; Chen. H.; Cummings, J.; Hughes, N. D.; Parsons, S.; Parkin, A.; Boyd, G.; Jodrell, D. I.; Sadler, P. J. *J. Med. Chem.* **2001**, *44*, 3616−3621.

(8) Aird, R. E.; Cummings, J.; Morris, R.; Ritchie, A. A.; Sadler, P. J.; Jodrell, D. I. *Br. J. Cancer* **2001**, *85* (suppl. 1 Jul), 101.

(9) Korn, S.; Sheldrick, W. S. *J. Chem. Soc., Dalton Trans.* **1997**, 2191−2199.

(10) Ren, J.; Jenkins, T. C.; Chaires, J. B. *Biochemistry* **2000**, *39*, 8439−8447.

(11) (a) Zunino, F.; Savi, G.; Pasini, A. *Cancer Chemother. Pharmacol.* **1986**, *18*, 180−182. (b) Pasini, A. *Gazz. Chim. Ital.* **1987**, *117*, 763−768.

(12) Bowler, B. E.; Ahmed, K. J.; Sundquist, W. I.; Hollis, L. S.; Whang, E. E.; Lippard, S. J. *J. Am. Chem. Soc.* **1989**, *111*, 1299−1306.

(13) Sundquist, W. I.; Bancroft, D. P.; Lippard, S. J. *J. Am. Chem. Soc.* **1990**, *112*, 1590−1596.

(14) Keck, M. V.; Lippard, S. J. *J. Am. Chem. Soc.* **1992**, *114*, 3386−3390.

(15) (a) Jennette, K. W.; Lippard, S. J.; Vassiliades, G. A.; Bauer, W. R. *Proc. Natl. Acad. Sci. U.S.A.* **1974**, *71*, 3839−3843. (b) Howe-Grant, M.; Wu, K. C.; Bauer, W. R.; Lippard, S. J. *Biochemistry* **1976**, *15*, 4339−4346.

(16) Farrell, N.; Ha, T. T. B.; Souchard, J.-P.; Wimmer, F. L.; Cros, S.; Johnson, N. P. *J. Med. Chem.* **1989**, *32*, 2240−2241.

(17) Farrell, N. *Met. Ions Biol. Syst.* **1996**, *32*, 603−639.

(18) Bierbach, U.; Qu, Y.; Hambley, T. W.; Peroutka, J.; Nguyen, H. L.; Doedee, M.; Farrell, N. *Inorg. Chem.* **1999**, *38*, 3535−3542.

(19) Zákovská, A.; Nováková, O.; Balcarová, Z.; Bierbach, U.; Farrell, N.; Brabec, V. *Eur. J. Biochem.* **1998**, *254*, 547−557.

(20) Bierbach, U.; Sabat, M.; Farrell, N. *Inorg. Chem.* **2000**, *39*, 1882−1890.

(21) He, Q.; Ohndorf, U.-M.; Lippard, S. J. *Biochemistry* **2000**, *39*, 14426−14435.

(22) Chen, Y.; Parkinson, J. A.; Guo, Z.; Brown, T.; Sadler, P. J. *Angew. Chem., Int. Ed.* **1999**, *38*, 2060−2063.

(23) Erkkila, K. E.; Odom, D. T.; Barton, J. K. *Chem. Rev.* **1999**, *99*, 2777−2795.

(24) Kielkopf, C. L.; Erkkila, K. E.; Hudson, B. P.; Barton, J. K.; Rees, D. C. *Nat. Struct. Biol.* **2000**, *7*, 117−121.

(25) (a) Reedijk, J. *Inorg. Chim. Acta* **1992**, *200*, 873−881. (b) Reedijk, J. *Chem. Commun.* **1996**, 801−806. (c) Jamieson, E. R.; Lippard, S. J. *Chem. Rev.* **1999**, *99*, 2467−2498.

(26) (a) Bau, R.; Sabat, M. In *Cisplatin-Chemistry and Biochemistry of a Leading Anticancer Drug*; Lippert, B., Ed.; Wiley-VCH: Weinheim, Germany, 1999; pp 318−337. (b) Takahara, P. M.; Rosenzweig, A. C.; Frederick, C. A.; Lippard, S. J. *Nature* **1995**, *337*, 649−652. (c) Admiraal, G.; Alink, M.; Altona, C.; Dijt, F. J.; van Garderen, C. J.; de Graaff, R. A. G.; Reedijk, J. *J. Am. Chem. Soc.* **1992**, *114*, 930−938. (d) Berners-Price, S. J.; Frey, U.; Ranford, J. D.; Sadler, P. J. *J. Am. Chem. Soc.* **1993**, *115*, 8649−8659.

Chart 1. Ligands and Complexes Studied in This Work and NMR Numbering Scheme (X = Cl or Guanine Derivatives, See Table 1)

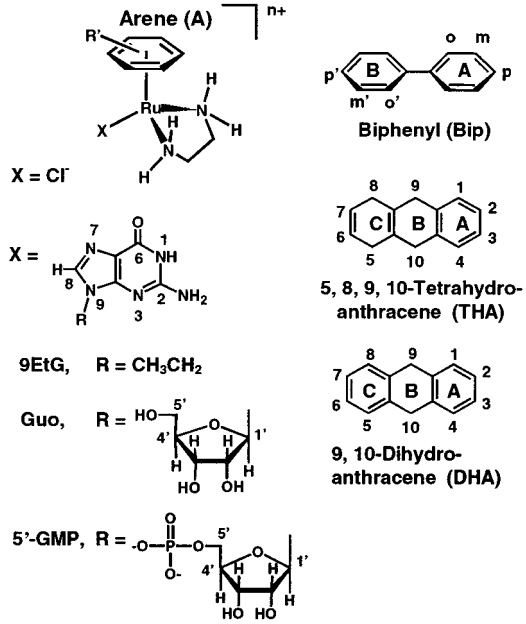

Table 1. Structural Studies of $[(\eta^6\text{-arene})Ru(en)(X)]^{n+}$ Complexes Reported in This Work[a]

arene	X	complex no.		structure[b]
Bip	Cl	**1**	X-ray	NOESY (DMF-d_6)[c]
	9EtG	**4**	X-ray	NOESY (acetone-d_6)[c]
	Guo	**5**	X-ray	NOESY (10% D_2O in H_2O)[c]
	5′-GMP	**8**[e]		NOESY (10% D_2O in H_2O)[c]
THA[f]	Cl	**2**	X-ray	NOESY (DMSO-d_6)[c]
	9EtG	**6**	X-ray	—[d]
	5′-GMP	**9**[e]		—[d]
DHA	Cl	**3**	X-ray	
	9EtG	**7**	X-ray	—[d]
	5′-GMP	**10**[e]		—[d]

[a] For structures and abbreviations, see Chart 1. [b] All crystals studied as PF_6^- salts. [c] Solvent for NMR. [d] Arene resonances too broad for NOESY studies. [e] Since the charge on 5′-GMP is dependent on pH, no overall charge is assigned to the 5′-GMP adducts discussed in this paper. [f] Note that in this paper free THA is referred to as 1,4,9,10-tetrahydroanthracene, whereas THA bound to Ru(II) is referred to as 5,8,9,10-tetrahydroanthracene, and that a different labelling scheme is used for the X-ray structures.

without further purification. $^{15}NH_2(CH_2)_2{}^{15}NH_2$ (^{15}N-en),[27] $[(\eta^6\text{-biphenyl})Ru(en)Cl]PF_6$ (**1**), and $[(\eta^6\text{-biphenyl})Ru(^{15}N\text{-en})Cl]PF_6$ (**^{15}N-1**) were synthesized as described previously.[7] Other ligands and complexes were prepared as described below.

Preparation of Ligands and Complexes. 1,4,5,8,9,10-Hexahydroanthracene ($C_{14}H_{16}$). 1,4,5,8,9,10-Hexahydroanthracene ($C_{14}H_{16}$) was prepared by reduction of anthracene (4.0 g, 22.4 mmol) with sodium in liquid ammonia according to the published procedure.[28] White needles (98% pure by ^{1}H NMR) were obtained in 37% yield by recrystallization first from benzene/chloroform (1:1), and then from benzene. ^{1}H NMR ($CDCl_3$): δ 5.68 (s, 4H), 2.51 (s, 8H), 2.37 (s, 4H).

1,4,9,10-Tetrahydroanthracene ($C_{14}H_{14}$). 1,4,9,10-Tetrahydroanthracene was prepared by reduction of 9,10-dihydroanthracene (5.0 g, 27.74 mmol) with lithium in liquid ammonia according to the published procedure[29] with some modification. White plates (97% purity by ^{1}H NMR) were obtained in 30% yield by recrystallization first from benzene, and then from acetone. ^{1}H NMR ($CDCl_3$): δ 7.11 (m, 4H), 5.78 (s, 2H), 3.25 (s, 4H), 2.70 (s, 4H).

$[(\eta^6\text{-}C_{14}H_{14})RuCl_2]_2$.[30] 1,4,5,8,9,10-Hexahydroanthracene (1.0 g, 5.43 mmol) was added to a solution of $RuCl_3{\cdot}3H_2O$ (0.84 g, 3.18 mmol) in dry ethanol (60 mL) and refluxed under Ar for 48 h. Filtration of the hot reaction mixture gave a yellow-brown solid which was washed with fresh ethanol (2 mL) followed by diethyl ether (4 × 10 mL) and dried under vacuum. Yield: 0.96 g (85.5%). ^{1}H NMR (DMSO-d_6): δ 5.83 (m, 2H), 5.71 (s, 2H), 5.61 (m, 2H), 3.21 (m, 2H), 3.05 (m, 2H), 2.5 (m, 4H).

$[(\eta^6\text{-}C_{14}H_{14})RuCl(en)][PF_6]$ (2). $[(\eta^6\text{-}C_{14}H_{14})RuCl_2]_2$ (0.205 g, 0.289 mmol) was stirred in dry methanol (25 mL) under Ar at 333 K. Ethylenediamine (48 μL, 0.72 mmol) was added in one portion. The reaction was stirred for 3 h and filtered, and NH_4PF_6 (0.4 g, 2.45 mmol) was added. The volume was reduced to ca. 6 mL on a rotary evaporator. After standing at 277 K overnight, a yellow microcrystalline precipitate formed, which was collected by filtration, washed with fresh methanol (0.5 mL), followed by diethyl ether (5 mL), and dried in vacuo. Yellow crystals suitable for X-ray diffraction were obtained by recrystallization from ethanol/ether. Yield: 0.1 g (32.9%). Anal. Calcd for $C_{16}H_{22}ClF_6N_2PRu$ (523.85): C, 36.68; H, 4.23; N, 5.35. Found: C, 36.20; H, 4.17; N, 5.34. ^{1}H NMR (DMSO-d_6): δ 6.29 (broad, 2H), 5.75 (s, 2H), 5.61 (m, 2H), 5.50 (m, 2H), 4.10 (broad, 2H), 3.18 (m, 4H), 2.62 (s, 4H), 2.32 (m, 2H), 2.23 (m, 2H).

$[(\eta^6\text{-}C_{14}H_{12})RuCl_2]_2$. 1,4,9,10-Tetrahydroanthracene (0.45 g, 2.47 mmol) was added to a solution of $RuCl_3{\cdot}3H_2O$ (0.48 g, 1.83 mmol) in dry ethanol (45 mL). The reaction was heated to reflux under Ar for 48 h. Filtration of the hot reaction mixture gave a brown solid which was washed with fresh ethanol (1 mL) followed by diethyl ether (4 × 10 mL) and dried under vacuum. Yield: 0.57 g (88.5%). ^{1}H NMR (DMSO-d_6): δ 7.27 (m, 4H), 5.89 (m, 4H), 3.92 (m, 4H).

$[(\eta^6\text{-}C_{14}H_{12})RuCl(en)][PF_6]$ (3). $[(\eta^6\text{-}C_{14}H_{12})RuCl_2]_2$ (0.10 g, 0.142 mmol) was stirred in dry methanol (10 mL) under Ar at 333 K. Ethylenediamine (24 μL, 0.36 mmol) was added in one portion. The reaction was maintained at 333 K with stirring for 5 h and filtered. The volume was reduced to ca. 4 mL with a rotary evaporator, and to this solution was then added a solution of NH_4PF_6 (0.20 g, 1.23 mmol) in methanol (2 mL). On shaking, a yellow solid precipitated. This mixture was allowed to stand overnight at 277 K. The precipitate was then collected by filtration, washed with fresh methanol (0.5 mL), followed by diethyl ether (5 mL), and dried under vacuum. Recrystallization from benzyl alcohol/ether gave yellow crystals suitable for X-ray diffraction studies. Yield: 0.1 g (67.5%). Anal. Calcd for $C_{16}H_{20}ClF_6N_2PRu$ (521.83): C, 36.82; H, 3.86; N, 5.37. Found: C, 36.50; H, 3.85; N, 5.38. ^{1}H NMR (DMSO-d_6): δ 7.20 (m, 4H), 6.19 (broad, 2H), 5.70 (m, 4H), 3.95 (m, 4H), 3.86 (broad, 2H), 2.22 (m, 2H), 2.05 (m, 2H).

$[(\eta^6\text{-biphenyl})Ru(en)(9EtG\text{-}N7)][PF_6]_2{\cdot}$(MeOH) (4). $[(\eta^6\text{-biphenyl})Ru(en)\text{-}Cl][PF_6]$ (**1**) (0.10 g, 0.20 mmol) was dissolved in water (30 mL), and 9EtG (37.63 mg, 0.21 mmol) was added. The mixture was stirred for 2 d at 313 K. After filtration, the volume was reduced to 8 mL, and then NH_4PF_6 (0.2 g, 1.23 mmol) was added. A precipitate was obtained overnight at 277 K. Recrystallization from methanol gave yellow crystals suitable for X-ray diffraction studies. Yield: 0.12 g (73.5%). Anal. Calcd for $C_{22}H_{31}F_{12}N_7O_2P_2Ru$ (816.55): C, 32.36; H, 3.83; N, 12.01. Found: C, 32.19; H, 3.80; N, 12.34.

$[(\eta^6\text{-biphenyl})Ru(en)(Guo\text{-}N7)][PF_6]_2{\cdot}3.75(H_2O)$ (5). $[(\eta^6\text{-biphenyl})Ru(en)(Guo\text{-}N7)][PF_6]_2{\cdot}3.75(H_2O)$ (**5**) was prepared by reacting $[(\eta^6\text{-biphenyl})Ru(en)Cl]PF_6$ (**1**) (89.7 mg, 0.18 mmol) with Guo (53.8 mg, 0.19 mmol) in water (20 mL) at 313 K for 4 d. The solution was filtered, and then NH_4PF_6 (0.16 g, 1.0 mmol) was added. After shaking, the reaction mixture was then kept at 277 K overnight. The precipitate was recrystallized from water. Slow evaporation of the aqueous solution gave yellow-green crystals suitable for X-ray diffraction studies.

(27) Zang, E.; Sadler, P. J. *Synthesis* **1997**, 410−412.
(28) Birch, A. J.; Fitton, P.; Smith, D. C. C.; Steere, D. E.; Stelfox, A. R. *J. Chem. Soc*. **1963**, 2209−2216.
(29) Harvey, R. G. *J. Org. Chem.* **1967**, *32*, 238−240.
(30) Beasley, T. J.; Brost, R. D.; Chu, C. K.; Grundy, S. L.; Stobart, S. R. *Organometallics* **1993**, *12*, 4599−4606.

Yield: 80.0 mg (46.5%). Anal. Calcd for $C_{24}H_{38.5}F_{12}N_7O_{8.75}P_2Ru$ (956.11): C, 30.15; H, 4.05; N, 10.60. Found: C, 30.17; H, 3.86; N, 10.42.

[(η^6-$C_{14}H_{14}$)Ru(en)(9EtG-*N7*)][PF_6]$_2$·(MeOH) (6). [(η^6-$C_{14}H_{14}$)Ru(en)Cl] [PF_6] (**2**) (70.68 mg, 0.14 mmol) was reacted with 9EtG (26.34 mg, 0.147 mmol) in water (30 mL) at 313 K for 2 d under Ar. The mixture was then filtered. The volume of the filtrate was reduced to 10 mL, and NH_4PF_6 (0.16 g, 1 mmol) was added. Yellow crystals suitable for X-ray diffraction studies were obtained on recrystallization of the precipitate from MeOH. Yield: 62.0 mg (52.4%). Anal. Calcd for $C_{24}H_{35}F_{12}N_7O_2P_2Ru$ (844.60): C, 34.13; H, 4.18; N, 11.61. Found: C, 34.28; H, 4.62; N, 11.96.

[(η^6-$C_{14}H_{12}$)Ru(en)(9EtG-*N7*)][PF_6]$_2$·2(MeOH) (7). [(η^6-$C_{14}H_{12}$)-Ru(en)Cl]-[PF_6] (**3**) (34.8 mg, 0.067 mmol) was reacted with 9EtG (12.0 mg, 0.067 mmol) in water (15 mL) at 313 K for 2 d under Ar. The mixture was then filtered. The volume of the filtrate was reduced to 4 mL, and NH_4PF_6 (0.16 g, 1 mmol) was added. Recrystallization of the precipitate from MeOH gave the yellow crystals suitable for X-ray diffraction studies. Yield: 32.5 mg (55.5%). Anal. Calcd for $C_{25}H_{37}F_{12}N_7O_3P_2Ru$ (874.63): C, 34.33; H, 4.26; N, 11.21. Found: C, 34.35; H, 4.55; N, 11.69.

Preparation of NMR Samples. [(η^6-biphenyl)Ru(en)(5′-GMP-*N7*)] (8). A solution containing this complex was prepared by mixing [(η^6-biphenyl)Ru(en)Cl][PF_6] (**1**) (2.43 mg, 4.9 μmol) with an aliquot (122.3 μL) of a stock solution of $Na_2$5′-GMP (40 mM) in 10% D_2O/90% H_2O (total volume 700 μL). This solution was kept at 310 K for 16 h. The final Ru concentration was 7.0 mM and pH 7.3. Then sodium trimethylsilyl[2,2,3,3-d_4]propionate (TSP, 2 μL of a 50 mM solution in D_2O) was added, and the solution was filtered into a 5 mm NMR tube.

[(η^6-biphenyl)Ru(^{15}N-en)(9EtG-*N7*)]$^{2+}$ (^{15}N-4), [(η^6-biphenyl)Ru(^{15}N-en)(Guo-*N7*)]$^{2+}$ (^{15}N-5), and [(η^6-biphenyl)Ru(^{15}N-en)(5′-GMP-*N7*)] (^{15}N-8). [(η^6-biphenyl)Ru(^{15}N-en)(9EtG-*N7*)]$^{2+}$ (**^{15}N-4**), [(η^6-biphenyl)Ru(^{15}N-en)(Guo-*N7*)]$^{2+}$ (**^{15}N-5**), and [(η^6-biphenyl)Ru(^{15}N-en)(5′-GMP-*N7*)] (**^{15}N-8**) were prepared by the following procedure. Typically, [(η^6-biphenyl)Ru(^{15}N-en)Cl][PF_6] (**^{15}N-1**) (1.77 mg, 3.55 mmol) and 9EtG (0.636 mg, 3.55 mmol) or Guo (1.0 mg, 3.55 mmol) or $Na_2$5′-GMP (88.75 μL of a 40.0 mM solution) were reacted in 10% D_2O/90% H_2O (total volume 700 μL) at 310 K for 24 h. The reaction was then complete, and the mixture was filtered directly into NMR tubes. For the spectra in acetone-d_6 or DMSO-d_6, the filtrate was lyophilized and then redissolved in acetone-d_6 or DMSO-d_6 (700 μL). The final Ru concentration was 5 mM.

[(η^6-$C_{14}H_{14}$)Ru(en)(9EtG-*N7*)]$^{2+}$ (6 and ^{15}N-6) and [(η^6-$C_{14}H_{14}$)-Ru(en)(5′-GMP-*N7*)] (9 and ^{15}N-9). [(η^6-$C_{14}H_{14}$)Ru(en)(9EtG-*N7*)]$^{2+}$ (**6** and **^{15}N-6**) and [(η^6-$C_{14}H_{14}$)Ru(en)(5′-GMP-*N7*)] (**9** and **^{15}N-9**) were prepared by in situ reactions of stoichiometric amounts of [(η^6-$C_{14}H_{14}$)-Ru(en)Cl][PF_6] (**2**) (0.91 mg, 1.73 μmol) and 9EtG (0.31 mg, 1.73 μmol) or $Na_2$5′-GMP (43.25 μL of a 40.0 mM solution)) in 10% D_2O/90% H_2O (total volume 680 μL). The mixture was degassed by bubbling Ar for 10 min, then sealed and kept at 310 K for 10 h. TSP (2 μL of a 50 mM solution in D_2O) was added, and the resulting mixture was filtered into NMR tubes under Ar. To prepare **^{15}N-6** and **^{15}N-9**, **^{15}N-2** was used. The final Ru concentration was 2.5 mM. The pH of solution was 6.3 for 9EtG adducts, and 7.4 for 5′-GMP adducts.

[(η^6-$C_{14}H_{12}$)Ru(en)(9EtG-*N7*)] (7) and [(η^6-$C_{14}H_{12}$)Ru(en)(5′-GMP-*N7*)] (10). [(η^6-$C_{14}H_{12}$)Ru(en)(9EtG-*N7*)] (**7**) and [(η^6-$C_{14}H_{12}$)-Ru(en)(5′-GMP-*N7*)] (**10**) were prepared by in situ reactions of [(η^6-$C_{14}H_{12}$)Ru(en)Cl][PF_6] (**3**) (0.98 mg, 1.88 μmol) and 9EtG (0.34 mg, 1.88 μmol) or $Na_2$5′-GMP (47.0 μL of a 40.0 mM solution) in 10% D_2O/90% H_2O (total volume 740 μL) at 310 K for 10 h; TSP (2 μL of a 50 mM solution in D_2O) was then added. The mixtures were filtered into NMR tubes under Ar. The final Ru concentration was 2.5 mM. The pH of the solution was 6.2 for complex **7**, and 7.1 for complex **10**.

Methods and Instrumentation. X-ray Crystallography. All diffraction data were collected using a Bruker (Siemens) Smart Apex ccd diffractometer equipped with an Oxford Cryosystems low-temperature device operating at 150 K. Absorption corrections for all data sets were performed with the multiscan procedure SADABS.[31] Structures were solved using either Patterson or direct methods (SHELXTL[32] or DIRDIF[33]); all except complex **5** were refined against F^2 using SHELXTL. For complex **2**, all H-atoms were located in a difference map and refined freely. In other structures, these atoms were placed in calculated positions, except those attached to nitrogen, which were refined freely. The difference in the strategy for H-atom treatment adopted for **2** was as a result of the rather unexpected nonplanarity of the hydrocarbon ligand; the H-atom positions were refined without difficulty, which gave confidence in the quality of the data set and the correctness of the model presented. We confirmed these structural features by repeating the structure determination of this compound using a different sample. All non-H atoms in all structures were modeled with anisotropic displacement parameters. In **4**, one of the crystallographically independent PF_6^- anions is disordered in an approximately 50:50 ratio about a common FPF axis. Similarity restraints were applied to the geometry and the displacement parameters for this ion.

The crystal structure of **5** was complicated by both twinning and pseudosymmetry effects. Several crystals were investigated, and all showed significant multiplicity. The diffraction patterns were indexed using the program GEMINI,[34] and a sphere of data was collected. An absorption correction was applied (assuming point group 1) by the multiscan procedure SADABS. The structure solved easily by direct methods, yielding the positions of a pair of centrosymmetrically related [Ru($C_{12}H_{10}$)(en)(Guo)] fragments and four PF_6^- anions, again in two centrosymmetrically related pairs. A rather noisy region of electron density was observed next to the N9 atoms of the guanine rings. The ribose sugar was used in a chirally pure form in the synthesis of this material, and so the space group *P*-1 is physically impossible. The true space group must be *P*1, but the difficulty in resolving the ribose fragments can be ascribed to the dominant effect on the phases of the centrosymmetric part of the structure. Two ribose fragments were eventually picked out of difference maps by ensuring that only peaks which corresponded to the known enantiomer of the sugar were selected. Further modeling revealed that while one pair of PF_6^- anions (based on P1 and P3) conforms closely to inversion symmetry, the other pair differs in orientation. At this stage, further difference peaks were assigned to water of crystallization, to give a conventional *R*-factor of 10%. It was clear at this stage that the centrosymmetric substructure could be constrained by applying the inversion relationship as part of the model. The advantage of this procedure is that it effectively cures ill-conditioning of the least squares and minimizes the number of parameters which needed to be refined against the rather weak data set obtained.[35] A refinement of this type was set up using the program CRYSTALS[36] for both fractional coordinates and displacement parameters. The ribose sugars, the PF_6^- anions based on P2 and P4, and the water molecules were all refined independently. Analysis of poorly fitting data at this stage revealed that most for which $F_o > F_c$ had $h = 0$; the program ROTAX[37] was used to identify the likely cause as twinning via a 2-fold rotation about the direct *a*-axis, which can be expressed by the matrix

(31) SADABS: Area-Detector Absorption Correction; Siemens Industrial Automation, Inc.: Madison, WI, 1996.
(32) Sheldrick, G. M. SHEXTL; Bruker Analytical X-ray Instruments: Madison, WI, 1995.
(33) Beurskens, P. T.; Beurskens, G.; Bosman, W. P.; de Gelder, R.; Garcia-Granda, S.; Gould, R. O.; Israel, R.; Smits, J. M. M. Crystallography Laboratory, University of Nijmegen, The Netherlands, 1996.
(34) Sparks, R.; Young, V.; Gemini; Bruker Analytical X-ray Instruments: Madison, Wisconsin, 2000.
(35) Watkin, D. *Acta Crystallogr*. **1994**, *A50*, 411−437.
(36) Watkin, D. J.; Prout, C. K.; Carruthers, J. R.; Betteridge, P. W.; Cooper, R. I. CRYSTALS Issue 11. Chemical Crystallography Laboratory, University of Oxford, Oxford, U.K., 1999.
(37) Cooper, R. I.; Gould, R. O.; Parsons, S.; Watkin, D. J. *J. Appl. Crystallogr*. **2002**, *35*, in press.

$$\begin{pmatrix} 1 & 0 & 0 \\ -0.045 & -1 & 0 \\ -0.200 & 0 & -1 \end{pmatrix}$$

This was confirmed by re-analysis of the diffraction pattern using GEMINI. This is clearly not a symmetry operation of the lattice, and it accounts for the difficulty encountered in indexing the diffraction pattern prior to data collection. A recently introduced feature of CRYSTALS allows this kind of twin matrix to be input directly without the need to split overlapping data manually. H-atoms attached to N and C were placed by conventional methods and re-idealized at the end of each refinement cycle. Coordinates for H-atoms attached to oxygen in the OH groups and water molecules were calculated using the program CALC-OH,[38] and thereafter allowed to ride on their parent atoms. Refinement was performed against F using 6014 data with $F > 4\sigma(F)$ and Chebychev polynomial weights.[39] The final R-factor was 6.65% (R_w = 6.95%) for 665 parameters. The final difference map showed no feature outwith ±1.8 e Å^{-3}. The twin scale factors refined to 0.66 and 0.44. The Flack parameter was not refined, but set at zero to avoid the need to model both nonmerohedral and racemic twinning; the known chirality of the sugar justifies this course of action.

In the tables of H-bonding data, esd's are given in cases where H-atom parameters have been refined.

NMR Spectroscopy. ^{1}H NMR spectra were acquired on either Bruker DMX 500 (^{1}H = 500 MHz) or Varian Unity INOVA (^{1}H = 600 MHz) NMR spectrometers using TBI [^{1}H,^{13}C,X] or triple resonance [^{1}H,^{13}C,^{15}N] probe-heads, respectively, and equipped with z-field gradients.

1D ^{1}H NMR spectra were typically acquired with 64 transients into 32 K data points over a spectral width of 6.0 kHz using a double pulsed-field gradient spin−echo pulse sequence. Typically, 2D [^{1}H,^{1}H] NOESY NMR spectra were acquired with 32 transients for each of 1024 t_1 increments (TPPI). The mixing time was 1 s, and the relaxation delay was 2 s. 2D [^{1}H,^{1}H] COSY and DQFCOSY spectra were acquired with 32 transients for each of 512 t_1 increments (States or TPPI). Water suppression was achieved by presaturation or by using a WATERGATE pulsed-field-gradient sequence.[40]

Both 1D ^{15}N-edited ^{1}H NMR spectra and 2D [^{1}H,^{15}N] HSQC NMR spectra (optimized for $^1J_{(NH)}$ = 73 Hz) were acquired using the sequence of Stonehouse et al.[41] A GARP decoupling sequence was used for ^{15}N decoupling during acquisition. Typically, 1D ^{1}H-{^{15}N} data were acquired with 16 transients into 1024 data points over a spectral width of 2.5 kHz (5.0 ppm) with a relaxation delay of 2.0 s. 2D [^{1}H,^{15}N] HSQC NMR data were acquired with four transients into 1024 data points over a ^{1}H (F2) spectral width of 2.5 kHz (5 ppm, centered at the water resonance) for each of 256 t_1 increments (TPPI), and over a ^{15}N (F1) spectral width of 0.76 kHz (15 ppm, center at −28 ppm) using a relaxation delay of 1.4 s between transients. Typically, 1D ^{1}H-{^{15}N} spectra were acquired over a 10 min period, and 2D [^{1}H,^{15}N] NMR HSQC spectra were acquired over a 30 min period.

^{31}P NMR spectra were obtained on either Bruker DMX 500 (^{31}P = 202 MHz) or Bruker DPX 360 (^{31}P = 146 MHz) NMR spectrometers at 298 K, using inverse-gated ^{1}H decoupling. Typical 1D ^{31}P-{^{1}H} NMR spectra at 202 MHz were acquired with 512 transients into 42 K data points over a spectral width of 40.7 kHz (200.8 ppm) using a relaxation delay of 1.3 s. Typical 1D ^{31}P-{^{1}H} NMR spectra at 146 MHz were acquired with 256 transients into 32 K data points over a spectral width of 14.6 kHz (100.28 ppm) using a relaxation delay of 0.5 s.

All data processing was carried out using XWIN NMR version 2.0 (Bruker U.K. Ltd.). ^{1}H NMR chemical shifts were internally referenced to 1,4-dioxane (3.77 ppm), or to the methyl singlet of TSP (0 ppm) in aqueous solutions, or to CD_2HCOCD_3 (2.06 ppm) in acetone-d_6 solution. ^{15}N resonances were referenced to 1 M $^{15}NH_4Cl$ in 1.5 M HCl (external) at 0 ppm, and ^{31}P resonances were referenced to 85% H_3PO_4 (external) at 0 ppm.

pH Measurement. The pH values of NMR samples in 10% D_2O/90% H_2O were measured at ca. 298 K directly in the NMR tube, before and after recording NMR spectra, using a Corning 240 pH meter equipped with an Aldrich micro combination electrode calibrated with Aldrich buffer solutions at pH 4, 7, and 10. The pH values of samples were adjusted with dilute solutions of HCl and NaOH. No correction has been applied for the effect of deuterium on the glass electrode.

Calculations of pK_a Values. The pH titration curves were fitted to the Henderson−Hasselbalch equation using the program KALEIDAGRAPH,[42] with the assumption that the observed chemical shifts are weighted averages according to the populations of the protonated and deprotonated species.

Results

We have studied the molecular structures of the parent chloro anticancer complexes [(η^6-arene)Ru(en)Cl][PF_6], where arene = biphenyl (Bip, complex **1**), 5,8,9,10-tetrahydroanthracene (THA, **2**), or 9,10-dihydroanthracene (DHA, **3**) (Chart 1), and those of their 9EtG, Guo, and 5′-GMP adducts, where possible both in the solid state and in solution (Table 1). The X-ray structure of complex **1** has been reported previously,[7] and those of **2** and **3** are reported here. We were successful in crystallizing yellow 9EtG and Guo adducts of {(η^6-biphenyl)Ru(en)}$^{2+}$ from MeOH and H_2O, respectively. The structures of the chloro-complex **1** and its 9EtG, Guo, and 5′-GMP adducts (**4**, **5**, and **8**) in solution were studied by NMR methods, including 2D [^{1}H,^{15}N] HSQC NMR using ^{15}N-en complexes, NOE measurements, pH and temperature dependences. For the anthracene derivatives, we were successful in crystallizing the 9EtG adducts **6** and **7**, but NMR work in solution was limited to 1D ^{1}H and 2D [^{1}H,^{15}N] HSQC NMR studies since broad resonances and slow chemical exchange processes complicated the interpretation of NOESY data.

X-ray Crystal Structures of Biphenyl Complexes. [(η^6-biphenyl)Ru(en)(9EtG-*N7*)][PF_6]$_2$·(MeOH) (4). In complex **4**, Ru(II) adopts the familiar "three-leg piano-stool" geometry. It is π-bonded to the hexadentate biphenyl ligand and σ-bonded to the N atoms of ethylenediamine and N7 of 9EtG (Figure 1). Crystallographic data are listed in Table 2, selected bond lengths and angles in Tables S1A and S1C, and selected H-bonding interactions in Table 3A. The propeller twist of the pendant phenyl with respect to the coordinated phenyl of the biphenyl ligand is 13.7°. The long axis of biphenyl is rotated away from the Ru−N7 vector by 136.0° (Table 4A) and therefore adopts the anti orientation with respect to the purine base. Atom O6 of 9EtG is strongly H-bonded to an en NH proton (H1B1) with a N1B···O6 distance of 2.761 Å and N1B−H1B1···O6 angle of 162.9° (Table 3A). Guanine-guanine pairing via two H-bonds between the G N2H and the G N3 (N2···N3 3.015 Å, N2−H2X···N3 172.0°, Figure 1) is present. In addition, for each molecule, the second G N2 proton (H2Y) together with the G N1 proton (H1X) forms two H-bonds to the O of MeOH (O1M) (N2···O1M 2.983 Å, N1···O1M 2.844 Å, Figure 1). One PF_6^- counteranion is beneath the guanine plane and H-bonded to an

(38) Nardelli, M. J. *Appl. Crystallogr.* **1999**, *32*, 563−571.
(39) Watkin, D. J.; Carruthers, J. R. *Acta Crystallogr.* **1979**, *A35*, 698−702.
(40) Piotto, M.; Saudek, V.; Sklenar, V. *J. Biomol. NMR* **1992**, *2*, 661−665.
(41) Stonehouse, J.; Shaw, G. L.; Keller, J.; Laue, E. D. *J. Magn. Reson., Ser. A* **1994**, *107*, 178−184.
(42) KALEIDAGRAPH, version 3.09; Synergy Software: Reading, PA, 1997.

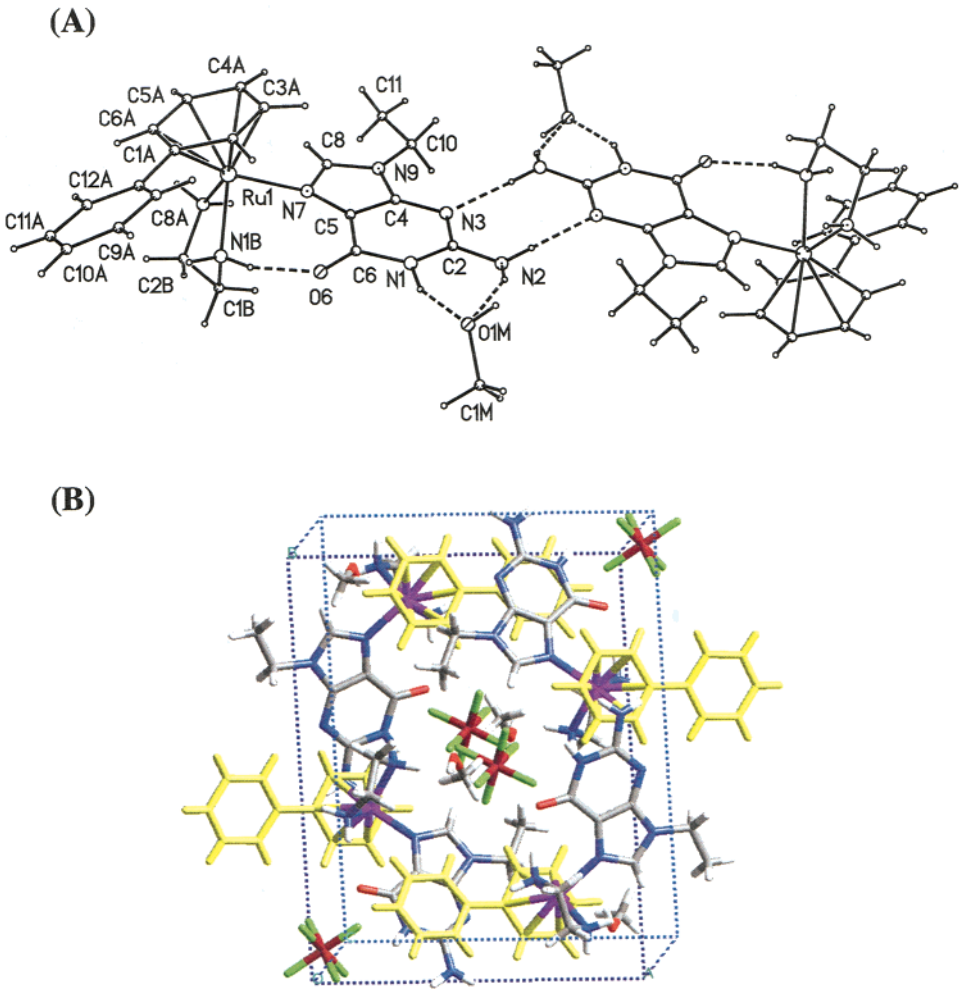

Figure 1. X-ray crystal structure of [(η^6-biphenyl)Ru(en)(9EtG-*N7*)][PF_6]$_2$·(MeOH) (**4**). (A) The H-bond network of the dimer. The atom numbering scheme is shown for one cation. PF_6^- ions are omitted for clarity. (B) Tetrameric aggregate in the unit cell (as viewed along the *c* axis). The core of this cyclic tetramer is filled by two PF_6^- ions and two MeOH molecules. The disordered PF_6^- ions are omitted for clarity. Two pendant phenyl rings inside the unit cell stack onto the purine bases of adjacent cations. Color code: Ru, purple; biphenyl, yellow; N, blue; O, red; C of G and MeOH, gray; H of G and MeOH, white; F, green; and P, dark red.

Table 2. Crystallographic Data for [(η^6-$C_{14}H_{14}$)Ru(en)Cl][PF_6] (**2**), [(η^6-$C_{14}H_{12}$)Ru(en)Cl][PF_6] (**3**), [(η^6-biphenyl)Ru(en)(9EtG-*N7*)][PF_6]$_2$·(MeOH) (**4**), [(η^6-biphenyl)Ru(en)(Guo-*N7*)][PF_6]$_2$·3.75(H_2O) (**5**), [(η^6-$C_{14}H_{14}$)Ru(en)(9EtG-*N7*)][PF_6]$_2$·(MeOH) (**6**), and [(η^6-$C_{14}H_{12}$)Ru(en)(9EtG-*N7*)][PF_6]$_2$·2(MeOH) (**7**)

	2	**3**	**4**	**5**	**6**	**7**
formula	$C_{16}H_{22}ClF_6N_2PRu$	$C_{16}H_{20}ClF_6N_2PRu$	$C_{22}H_{31}F_{12}N_7O_2P_2Ru$	$C_{24}H_{38.5}F_{12}N_7O_{8.75}P_2Ru$	$C_{24}H_{35}F_{12}N_7O_2P_2Ru$	$C_{25}H_{37}F_{12}N_7O_3P_2Ru$
molar mass	523.85	521.83	816.55	956.11	844.60	874.63
crystal system	monoclinic	orthorhombic	monoclinic	triclinic	monoclinic	triclinic
space group	$P2_1/n$	*Pbca*	$P2_1/n$	*P*1	$P2_1/n$	*P*-1
color	orange	yellow	yellow	yellow	pale yellow	yellow
a/Å	12.171(3)	11.1220(18)	13.2927(14)	8.850(3)	16.6279(11)	10.6486(17)
b/Å	8.4733(18)	12.576(2)	15.9583(17)	11.543(4)	9.0528(6)	12.317(2)
c/Å	18.946(4)	25.593(4)	15.0878(16)	17.556(5)	21.5446(15)	13.006(2)
α/deg	90	90	90	103.254(4)	90	73.957(2)
β/deg	103.854(3)	90	108.613(2)	92.885(4)	99.677(1)	79.483(2)
γ/deg	90	90	90	90.983(4)	90	84.977(2)
T/K	150(2)	150(2)	150(2)	150(2)	150(2)	150(2)
Z	4	8	4	2	4	2
R [$F > 4\sigma(F)$][a]	0.0230	0.0444	0.0895	0.0665	0.0593	0.0291
R_w[b]	0.0625	0.1055	0.220	0.0695[d]	0.1391	0.0768
GOF[c]	1.062	1.038	1.222	0.981	1.132	1.035
$\Delta\rho$ max and min /e Å^{-3}	+0.722, −0.371	2.328, −2.190	2.00, −1.21	1.76, −1.84	1.12, −0.80	0.56, −0.45

[a] $R = \sum||F_o| - |F_c||/\sum|F_o|$. [b] $R_w = [\sum w(F_o^2 - F_c^2)^2/\sum wF_o^2)]^{1/2}$. [c] GOF = $[\sum w(F_o^2 - F_c^2)^2/(n-p)]^{1/2}$, where n = number of reflections, and p = number of parameters. [d] Based on F for structure **5**.

en NH proton (H2B2, N2B···F4 2.952 Å); the second PF_6^- ion (disordered) is above the guanine plane, and its presence prevents intramolecular arene-purine stacking.

In one unit cell, four molecules form a cyclic aggregate when viewed along the *c* axis (see Figure 1B). The core of this cyclic tetramer is filled by two PF_6^- ions and two solvent CH_3OH

Table 3. Selected H-Bonding Interactions for Complexes **4**, **5**, **6**, and **7** (O1M Is MeOH Oxygen)

(A) Complex **4** [(η^6-biphenyl)Ru(en)(9EtG-*N7*)][PF_6]$_2$·(MeOH)

D–H···A	H···A (Å)	D···A (Å)	∠D–H···A (deg)
N1B−H1B1···O6 (intra)	1.868	2.761(8)	162.91
N2−H2X···N3 (inter)	2.123	3.015(9)	171.96
N2−H2Y···O1M	2.168	2.983(12)	151.25
N1−H1X···O1M	2.004	2.844(11)	155.19

(B) Complex **5** [(η^6-biphenyl)Ru(en)(Guo-*N7*)][PF_6]$_2$·3.75(H_2O) (Cations I and II)

cation I				cation II			
D–H···A	H···A (Å)	D···A (Å)	∠D–H···A (deg)	D–H···A	H···A (Å)	D···A (Å)	∠D–H•••A (deg)
N14−H141···O61 (intra)	1.8899	2.799(8)	158.97	N18−H181···O65 (intra)	1.8899	2.799(8)	158.97
N14−H142···O65(II) (inter)	2.5454	3.212(7)	127.28	N18−H182···O61(I) (inter)	2.5454	3.212(7)	127.28
N24−H241···O52	2.7750	3.714(7)	169.28	N28−H281···O69(W)	2.1963	3.083(13)	154.72
N11−H11···O29(W)	1.9772	2.841(16)	150.65	N15−H15···O19(W)	2.0708	2.949(16)	153.63
N21−H212···O29(W)	2.0335	2.861(17)	144.66	N25−H252···O19(W)	2.2352	3.050(16)	143.47
N21−H211···O99(W)	2.2411	3.136(17)	156.44	N25−H251···O32(I) (inter)	1.7916	2.715(11)	162.79

(C) Complex **6** [(η^6-$C_{14}H_{14}$)Ru(en)(9EtG-*N7*)][PF_6]$_2$·(MeOH)

D–H···A	H···A (Å)	D···A (Å)	∠D–H···A (deg)
N1B−H1B1···O6 (intro)	1.919	2.812(4)	163.30
N2−H2X···N3 (inter)	2.349	3.105(4)	168.07
N2−H2Y···O1M	2.403	3.085(5)	142.04
N1−H1X···O1M	2.161	2.829(6)	160.84

(D) Complex **7** [(η^6-$C_{14}H_{12}$)Ru(en)(9EtG-*N7*)][PF_6]$_2$·2(MeOH)

D–H···A	H···A (Å)	D···A (Å)	∠D–H···A (deg)
N1B−H1NB···O6 (intro)	2.081	2.840(2)	163.09
N1B−H1NA···O6 (inter)	2.237	3.031(2)	146.19
N2−H2X···N3 (inter)	2.299	3.085(3)	162.19
N2B−H2NA···O1M	2.112	2.895(3)	162.50

Table 4. Comparison of the Conformations of Guanine Adducts and Their Parent Chloro-Complexes (see Figures 6 and 7) (X = Cl or N7 of G)

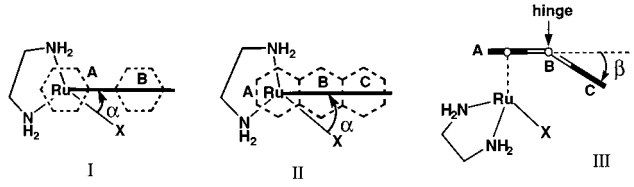

(A) Biphenyl Complexes **1**, **4**, and **5**

	1 (Cl)	**4** (9EtG)	**5** (Guo)
Bip orientation, α (I), [Δα],[b] (deg)	26.8(2)	136.0(3) [+109.2]	13.2(3) [−13.6]
Bip propeller twist, χ,[α] [Δχ],[b] (deg)	26.2(4)	13.7(5) [−12.5]	17.9(4) [−8.3]
ring B−G distance (Å)/dihedral angle (deg)		4.022(5)/4.48(5) (inter)[c]	3.801(4)/23.8(4) (intra)[c] 4.199(4)/23.0(6) (inter)[e]

(B) THA Complexes **2** and **6** and DHA Complexes **3** and **7**

	2 (Cl)	**6** (9EtG)	**3** (Cl)	**7** (9EtG)
THA/DHA orientation, α (II), [Δα],[g] (deg)	45.12(6)	25.62(14) [−19.5]	64.09(8)	20.88(7) [−43.2]
hinge bending angle, β (III),[f] [Δβ],[g] (deg)	−7.53(12)	+27.8(2) [+35.33]	+40.65(16)	+31.95(9) [−8.7]
ring C−G distance (Å)/dihedral angle (deg)		3.447(9)/3.30(17) (intra)[h]		3.310(12)/3.07(8) (intra)[h]

[a] χ: Twist of pendant phenyl ring (B) with respect to coordinated phenyl (A) of Bip. [b] The change of torsion angles for **4** and **5** as compared to **1**. [c] Ring B and six-membered ring of G of an adjacent cation. [d] Ring B and five-membered ring of G of the same cation. [e] Ring B with six-membered ring of G of an adjacent cation. [f] The hinge is defined by C7A−C10A, see Figures 3 and 4. A + ve sign for β indicates movement toward Ru−X. [g] The change of torsion angles for **6** and **7** as compared to **2** and **3**, respectively. [h] Ring C and purine ring of G of the same cation.

molecules. The pendant phenyl ring stacks onto the purine base of an adjacent cation with a centroid−centroid separation of 4.0 Å and a dihedral angle of 4.5° (see space-filling model in Figure S1A). Tetramers are stacked on top of one another along the *c* axis. In the same layer, tetramers are connected by four sets of base pairs via H-bonds N2−H2X···N3 along *a* and *b* axes. Figure 1A shows base-pairing along the *b* axis.

[(η^6-biphenyl)Ru(en)(Guo-*N7*)][PF_6]$_2$·3.75H_2O (5). [(η^6-biphenyl)Ru(en)(Guo-*N7*)][PF_6]$_2$·3.75H_2O (**5**) crystallizes with two independent [(η^6-biphenyl)Ru(en)(Guo-*N7*)]$^{2+}$ cations (I and II, Figure 2) in the asymmetric unit, which also contains four PF_6^- counterions and nine water molecules (three with half-occupancy). The structures of these two cations differ significantly only in the orientation of the ribose ring. Selected bond

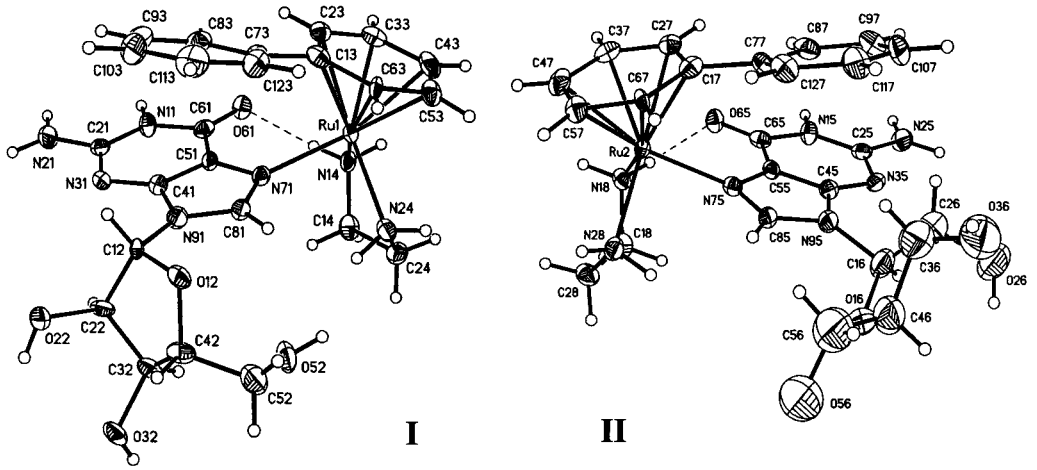

Figure 2. Two independent cations (I and II) of [η^6-biphenyl)Ru(en)(Guo-*N7*)]$^{2+}$ in the asymmetic unit of the X-ray structure of complex **5**, showing the atom numbering scheme and 30% probability thermal ellipsoids. H-bonding interactions of en NH with G O6 are indicated by dotted lines.

lengths and angles are listed in Tables S1A and S1C. The torsion angles $\upsilon_0-\upsilon_4$ and the pseudorotational parameters P and ϕ_m for the ribose ring characterize the ring conformation[43] and are listed in Table S2. In both these cations, the sugar puckers take the N-type (C2′-exo/C3′-endo) conformation ($P = -12.69°$ for cation I and $-12.17°$ for cation II).

The long axis of the biphenyl ligand is rotated away from the Ru−N7 vector by 13.2°. The propeller twist of biphenyl is 17.9° (Table 4A). When viewed normal to the plane of the purine base (Figure 7B), there is overlap of the pendant phenyl ring with the purine five-membered ring (distance 3.8 Å, dihedral angle 23.8°, Table 4A). The six-membered ring of the same purine stacks with a pendant phenyl ring of an adjacent cation (distance 4.2 Å, dihedral angle 23.0°, Table 4A). Thus the pendant phenyl ring is stacked alternately with the purine five-membered and six-membered rings to form a columnar-type structure (as viewed down *c*, see Figure S1B).

Selected H-bonds for **5** are listed in Table 2B. For cations I and II, there is strong intramolecular H-bonding between an en NH and G O6, N14···O61(I) (N18···O65(II)) distance of 2.799 Å, and N14−H141···O61(I) (N18−H181···O65(II)) angle of 159.0°. Intermolecular base-pairing between guanine bases of **5** is absent. Instead, N2H, N3, and N1H of Guo are H-bonded to PF_6^- and H_2O. Most of the water molecules and PF_6^- ions are within H-bonding distances to the NH groups of en or O(5′), O(3′), O(2′), and O(1′) atoms of the ribose ring, and thus form a complicated H-bonding network (possible H-bonding interactions involving water molecules and ribose are listed in Table S3).

X-ray Crystal Structures of THA and DHA Complexes. [(η^6-$C_{14}H_{14}$)Ru(en)Cl][PF_6] (2) and [(η^6-$C_{14}H_{12}$)Ru(en)Cl]-[PF_6] (3). The structures of the cations of **2** and **3** are shown in Figure 3. The crystallographic data are listed in Table 2, and selected bond lengths and angles are in Tables S1B and S1D. In the THA ($C_{14}H_{14}$) complex **2**, the tricyclic ring system is nearly flat. The outer ring (C) is slightly bent up away from the Cl ligand about the C7A−C10A hinge by 7.5°. The long axis through the THA ligand is rotated away from the Ru−Cl vector by 45.1° (Table 4B). In the DHA ($C_{14}H_{12}$) complex **3**, the tricyclic ring system deviates significantly from planarity.

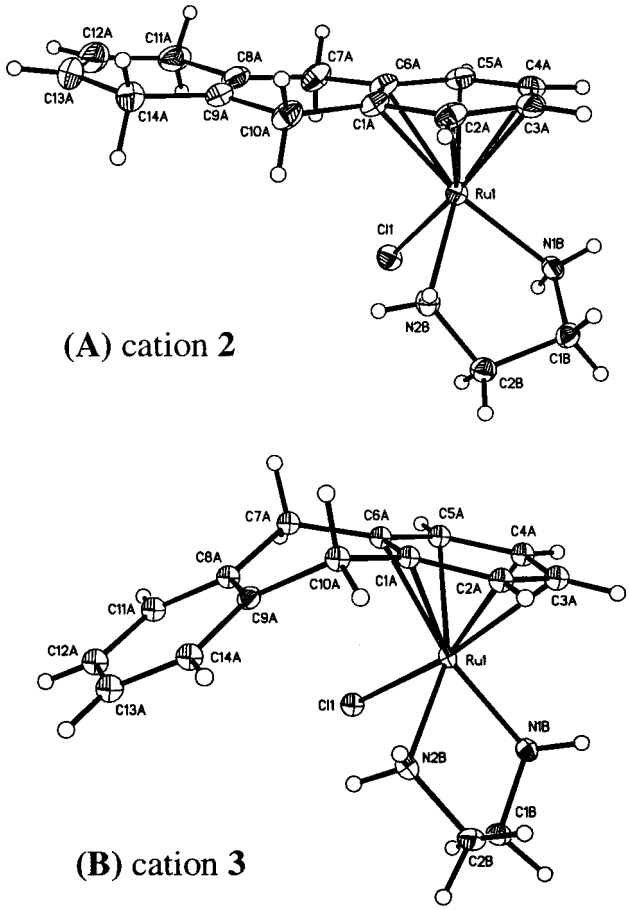

Figure 3. X-ray structures and atom numbering schemes for (A) [(η^6-$C_{14}H_{14}$)Ru(en)Cl]$^+$ in complex **2**, and (B) [(η^6-$C_{14}H_{12}$)Ru(en)Cl]$^+$ in complex **3**, at 30% probability thermal ellipsoids.

The outer ring (C) is bent down toward the Cl ligand about the C7A−C10A hinge by 40.6°. The long axis of DHA is rotated away from the Ru−Cl vector by 64.1° (Table 4B). In both complexes, there are H-bonding interactions between NH protons of en and F atoms of PF_6^- ions. No intermolecular arene ring stacking is observed for either complex.

[(η^6-$C_{14}H_{14}$)Ru(en)(9EtG-*N7*)][PF_6]$_2$ (MeOH) (6) and [(η^6-$C_{14}H_{12}$)Ru(en)-(9EtG-*N7*)][PF_6]$_2$·2(MeOH) (7). Both of these crystal structures show the presence of strong intramolecular

(43) Saenger, W. *Principles of Nucleic Acid Structure*; Springer-Verlag: New York, 1985.

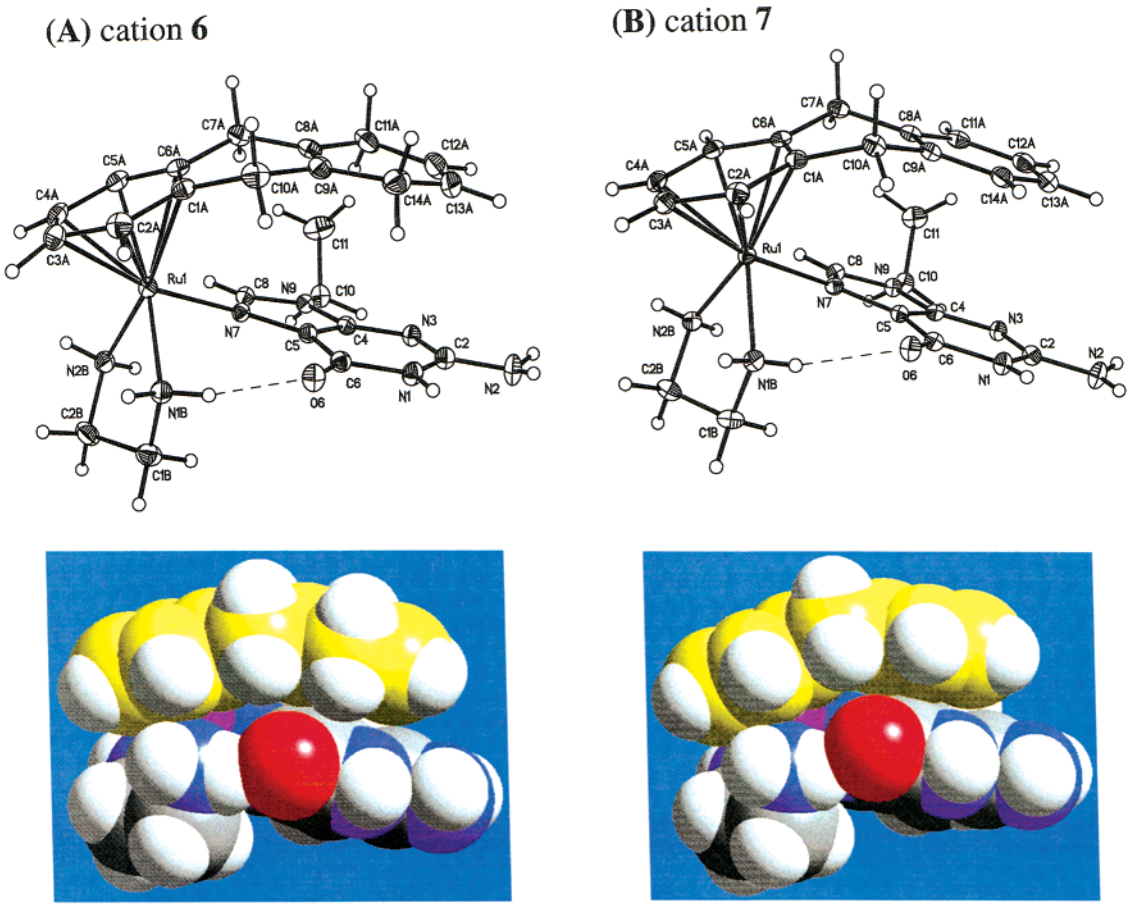

Figure 4. X-ray structures and atom numbering schemes for (A) $[(\eta^6\text{-}C_{14}H_{14})Ru(en)(9EtG\text{-}N7)]^{2+}$ in complex **6**, and (B) $[(\eta^6\text{-}C_{14}H_{12})Ru(en)(9EtG\text{-}N7)]^{2+}$ in complex **7**, at 30% probability thermal ellipsoids. The space-filling models clearly show the intramolecular arene-guanine base stacking and H-bonding interactions between en NH and G O6. Color code: C of $C_{14}H_{14}$ and $C_{14}H_{12}$, yellow; C of 9EtG and en, gray; Ru, purple; O, red; N, blue; and H, white.

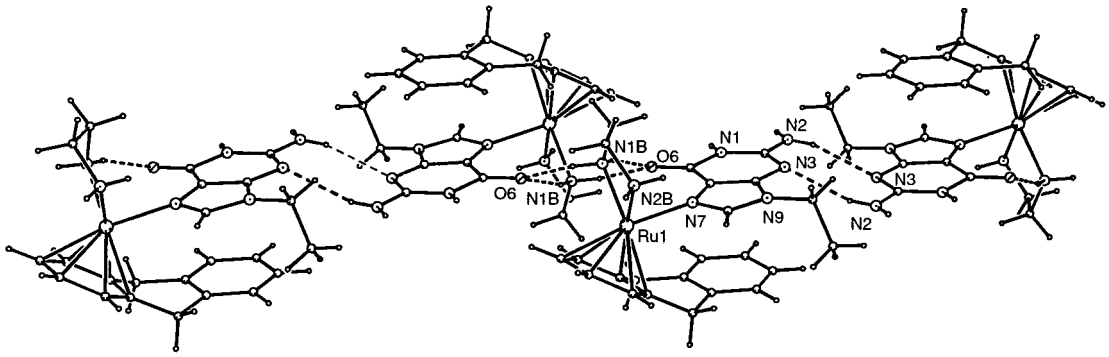

Figure 5. The helical chain-type structure of $[(\eta^6\text{-}C_{14}H_{12})Ru(en)(9EtG\text{-}N7)][PF_6]_2\cdot 2(MeOH)$ (**7**) (along the *c* axis), showing guanine−guanine base pairing via N2−H···N3, intramolecular H-bonding between en NH and G O6, intermolecular H-bonding between en NH and G O6, and the intramolecular outer arene ring-guanine base stacking. PF_6^- ions and MeOH molecules are omitted for clarity.

$\pi-\pi$ arene-nucleobase stacking. As can be seen in Figure 4, the outer ring (C) of THA/DHA lies directly over the purine base (see also Figure 7C and D). The centroid−centroid separation between ring C and the purine ring is 3.45 Å for **6** and 3.31 Å for **7**, with dihedral angles of 3.3° and 3.1°, respectively (Table 4B). Ring C is bent down toward the purine about the C7A−C10A hinge by 27.8° in **6**, and by 31.9° in **7**. The long axes of THA (**6**) and DHA (**7**) are rotated away from the Ru−N7 vectors by 25.6° and 20.9°, respectively. There is intramolecular H-bonding between en NH and G O6 (N1B···O6 2.812 Å and N1B−H1B1···O6 163.3° for **6**, N1B···O6 2.840 Å and N1B−H1NB···O6 163.1° for **7**, Table 3C and D). Additionally for **7**, the second H atom (H1NA) on the same en N1B is H-bonded to O6 of a neighboring G base (Figure 5) with an N1B···O6 distance of 3.031 Å. For both structures, dimers are formed via a pair of H-bonds between G N2H and G N3 (N2···N3 3.105 Å for **6**, 3.085 Å for **7**). For **6**, the second G N2H proton (H2Y) together with a G N1H proton (H1X) form two H-bonds to O of MeOH (N2···O1M 3.085 Å, N1···O1M 2.829 Å, Figure S2). No intermolecular arene-base ring stacking is observed for complexes **6** or **7**.

NMR Structures of Biphenyl Complexes in Solution. [(η^6-biphenyl)Ru(en)Cl][PF_6] (1) in DMF-d_6. The ^{1}H NMR spectrum of complex **1** at 298 K was assigned using 2D COSY

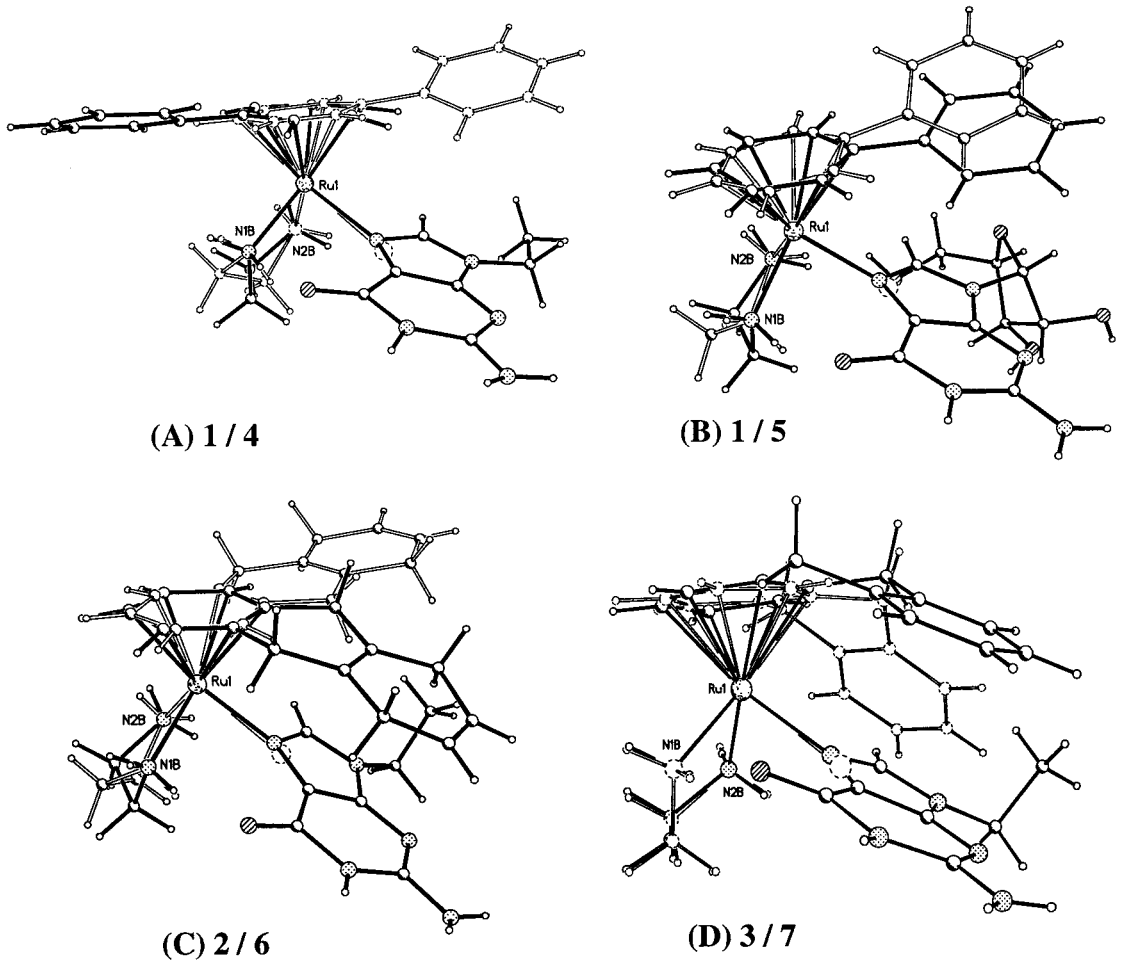

Figure 6. Comparison of the conformations of the parent chloro-complexes $[(\eta^6\text{-arene})\text{Ru(en)Cl}]^+$ (light line) and the guanine adducts $[(\eta^6\text{-arene})\text{Ru(en)(G-}N7\text{)}]^{2+}$ (heavy line). Arene = Bip in (A) and (B), THA in (C), and DHA in (D); guanine derivative = 9EtG in (A), (C), and (D), Guo in (B). Alignments are based on a superposition of the labeled atoms (Ru1, N1B, and N2B of en). In each case there is a significant reorientation of the arene with respect to the parent chloro-complex, resulting in arene−nucleobase interaction.

(Figure S3**)** and NOESY ^{1}H NMR spectroscopy (Figure 8). The aromatic resonances are divided into two groups: the high-field resonances (δ 6.28, 6.08, and 5.98) corresponding to the protons H(o), H(p), and H(m) of the coordinated phenyl ring (A), and the low-field resonances (δ 7.86 and 7.52) corresponding to the protons H(o′), H(m′), and H(p′) of the pendant phenyl ring (B) (H(m′) and H(p′) overlap at δ 7.52). The strong NOE between H(o′) and H(o) is in accordance with the distance of 2.2 Å determined for the X-ray crystal structure of **1**.[7] Only one resonance is observed for the ortho protons and one for the meta protons.

The four en NH protons give rise to two broad resonances at δ 6.72 and 4.26. These are assigned to the two types of protons on the same N: NH(u1, u2) (δ 6.72) which point up toward ring A, and NH(d1, d2) (δ 4.26) which point down away from ring A.[44] NH(u1, u2) show NOEs to H(o), H(m), and H(p) of ring A with medium intensity as compared with the NOE of NH(u)−NH(d), while the NOEs between NH(d1, d2) and the ring A protons are very weak. These NOE intensities ($\propto 1/r^6$) are in accordance with the crystal structure of **1**[7] in which the biphenyl ligand is in the syn orientation with respect to the Cl ligand (α = 26.8°, see Table 4A and Figure 6). The average distances of NH(u1, u2) protons to H(o), H(m), and H(p) are 3.65, 3.54, and 2.71 Å, respectively, while the average distances of NH(d1, d2) protons to H(o), H(m), and H(p) are longer, 3.84, 3.71, and 4.41 Å, respectively.

$[(\eta^6$-biphenyl)Ru(en)(9EtG-*N7*)$][PF_6]_2\cdot$(MeOH) (4) in Acetone-d_6. Crystalline complex **4** is poorly soluble in water, and therefore [^{1}H, ^{1}H] 2D NMR spectra were acquired for acetone-d_6 solutions.^{1}H NMR signal assignments were obtained from 2D DQFCOSY (Figure S4) and NOESY (Figure 9) ^{1}H NMR data. As compared to the parent chloro-complex **1** in DMF-d_6, the signal for the NH(d1, d2) protons of **4** was surprisingly broad and low-field shifted to δ 5.34, whereas the signal for NH(u1, u2) protons at δ 6.49 was relatively sharp. These assignments for en-NH protons were confirmed by the 2D [^{1}H, ^{15}N] HSQC NMR spectrum of **^{15}N-4** in acetone-d_6 solution. Correlations between NH(u1, u2) and en CH_2CH_2 were observed in the DQFCOSY NMR spectrum (Figure S4), but cross-peaks for NH(d1, d2) correlations with en CH_2CH_2 were too broad to detect. The NOE cross-peak between NH(d1, d2) and NH(u1, u2) was broad, but observable. NOEs were observed between the ethyl protons of 9EtG and H(m′), H(o′), and H(p′) of ring

(44) The two N atoms of en are equivalent since there is a symmetry plane through the long axis of biphenyl and Ru. The inequivalence of the two protons on the same N arises from the ring-current effect of the coordinated biphenyl. The NH(d1, d2) protons are within the ring-current cone of the phenyl ring and are thus greatly shielded (δ 4.26), whereas the NH(u1, u2) protons are outside the cone and are thus relatively deshielded (δ 6.72).

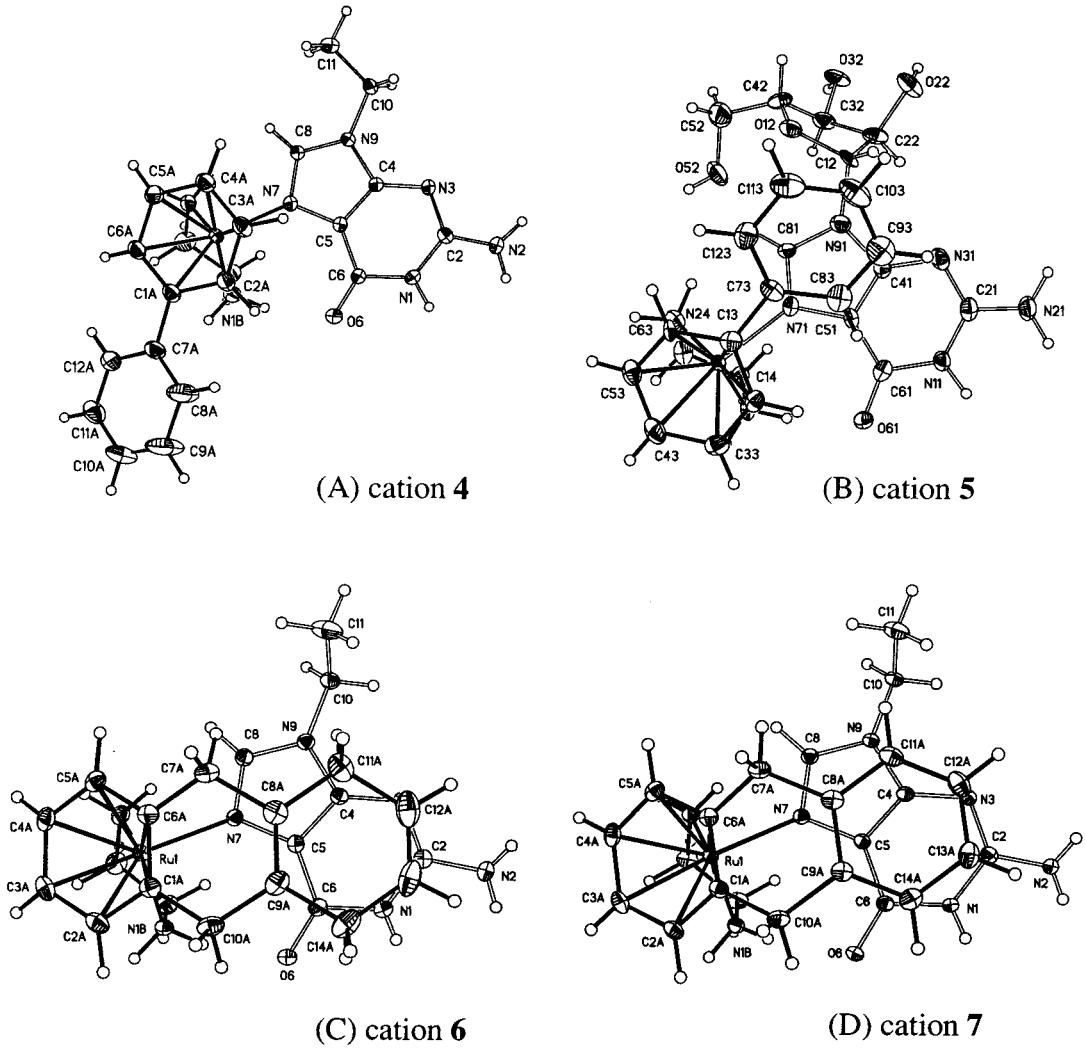

Figure 7. Projections of the structures of cations. (A) [(η^6-biphenyl)Ru(en)(9EtG-*N7*)]$^{2+}$ (**4**), (B) [(η^6-biphenyl)Ru(en)(Guo-*N7*)]$^{2+}$ (**5**), (C) [(η^6-$C_{14}H_{14}$)-Ru(en)(9EtG-*N7*)]$^{2+}$ (**6**), and (D) [(η^6-$C_{14}H_{14}$)Ru(en)(9EtG-*N7*)]$^{2+}$ (**7**) (30% probability thermal ellipsoids), showing arene (heavy line)-guanine base (light line) stacking in (B), (C), and (D) with the arene rings syn to G bases, whereas in (A), the arene ring is anti to the G base.

B (Figure 9B). These, together with NOEs between H8 and H(o′)/H(o), and between NH(u1, u2) and H(p) (Figure 9A), indicate that a syn conformation predominates for the pendant phenyl ring (B) with respect to the G base. Also, the presence of NOEs between H8 and NH(d1, d2) (broad) and the absence of NOE cross-peaks between H8 and NH(u1, u2) suggest that H8 of 9EtG points toward NH(d1, d2). The cross-peaks NH-(d1, d2) in the 2D [^{1}H,^{15}N] HSQC NMR spectrum of **^{15}N-4** in DMSO-d_6 solution sharpened as the temperature was raised from 295 to 310 K, Table S7.

[(η^6-biphenyl)Ru(en)(Guo-*N7*)]$^{2+}$ (5) in Aqueous Solution. 2D NOESY and DQFCOSY ^{1}H NMR spectra of complex **5** in 10% D_2O/90% H_2O at 298 K were used to assign the proton resonances (Tables S4 and S5). In contrast to the parent chloro-complex **1** in DMF-d_6, the en NH(d1, d2) signals for **5** were too broad to detect at ambient temperature, but the NH(u) signals were reasonably sharp (as for **4**). The 2D [^{1}H,^{15}N] HSQC NMR spectrum for **^{15}N-5** at 298 K contained two cross-peaks for NH-(u1, u2) at δ 6.51/−29.38 and δ 6.55/−28.87, but no cross-peaks for NH(d1, d2) (see Table S7). When the temperature was raised to 328 K, broad peaks for NH(d1, d2) appeared. At this temperature, the four cross-peaks at δ 6.45/−29.1, 4.98/−29.1, 6.48/−28.62, and 4.65/−28.62 can be assigned to NH-(u1), NH(d1), NH(u2), and NH(d2), respectively (Figure S6A and Table S7). In contrast to complexes **1** and **4**, the two ^{15}N atoms of en in **5** are magnetically nonequivalent, as expected in view of the chirality of the sugar. Yet as for **1** and **4**, only one resonance is observed for the ortho protons and one for the meta protons. This is probably due to fast rotation of the biphenyl ligand about the arene-Ru π-bond together with fast propeller twisting on the NMR time scale. A series of 2D [^{1}H,^{15}N] HSQC NMR spectra of **^{15}N-5** in DMSO-d_6 was also acquired at various temperatures (Table S7). The NH(d1, d2) resonances were also too broad to detect at 298 K in this solvent but appeared when the temperature was raised to 310 K. The similarity of the results for DMSO-d_6 and aqueous solutions suggests that overlap with the water resonance is not the reason why the NH(d1, d2) resonances of **5** are unobservable in aqueous solution at low temperature.

In the 2D NOESY ^{1}H NMR spectrum of **5** (Figure 10), NOEs were observed for H8−H(o′), H8−H(o), NH(u1, u2)−H(m), and NH(u1, u2)−H(p), indicating that the syn conformation predominates for ring B with respect to the G base. A similar orientation for ring B occurs in the crystal structure, and the

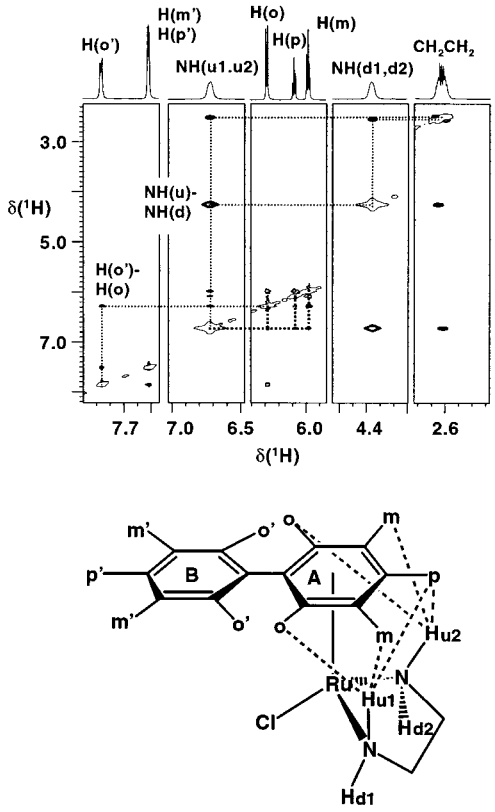

Figure 8. Top: 2D NOESY ^{1}H NMR spectrum of [(η^6-biphenyl)Ru(en)Cl]$^+$ (**1**) in DMF-d_6 at 298 K. Bottom: Structure with interligand NOEs indicated by dotted lines.

observed NOEs are in agreement with the average crystallographic distances of NH(u1, u2)−H(m) 2.70 Å, NH(u1, u2)−H(p) 3.37 Å, NH(u1, u2)−H(o) 4.73 Å, H8−H(o) 3.35 Å, H8−H(o′) 3.82 Å, H8−H(m) 4.68 Å, H8−H(m′) 4.81 Å, H8−H(p) 5.85 Å, and H8−H(p′) 5.40 Å. The NOE cross-peaks for H8−H1′, H8−H2′, H8−H3′, and H8−H4′ have intensity ratios of ca. 5:1:1:1, respectively (Figure S5A). The strong NOE for H8−H1′ observed in this spectrum suggests that a syn orientation predominates for the G base with respect to the ribose ring. This conformational feature is different from the solid state where an anti orientation was found for **5**. The value of ^3J (H1′/H2′) = 4.49 Hz is lower than that for free Guo (6.05 Hz), suggesting that the sugar conformation changes when Guo binds to Ru.

[(η^6-biphenyl)Ru(en)(5′-GMP-*N7*)] (8) in Aqueous Solution. 2D NOESY and DQFCOSY ^{1}H NMR spectra of **8** in 10% D_2O/90% H_2O at 310 K were used to assign the proton NMR resonances (Tables S4 and S5). The four en NH resonances at δ 6.36, 5.27, 6.39, and 5.09 can be assigned to NH(u1), NH(d1), NH(u2), and NH(d2), respectively. All are of reasonable intensity at this temperature. Their assignments were confirmed by reference to the 2D [^{1}H,^{15}N] HSQC ^{1}H NMR spectrum of **^{15}N-8** (Figure S6B). The inequivalence of en NH_2 can be accounted for by the chirality of the sugar ring of 5′-GMP. Only one resonance is observed for the ortho protons and one for the meta protons of biphenyl, as for **5**. In the 2D NOESY NMR spectrum (Figure 11), the NOE cross-peaks for H8−H(o′), H8−H(o), and NH(u1, u2)−H(p) indicate that the syn conformation predominates for the biphenyl ring with respect to the G base. There are NOEs between H8 and NH(d1, d2), but not between H8 and NH(u1, u2), suggesting that H8 of G points toward NH(d1, d2). The ratio of the intensities of the NOE cross-peaks H8−H1′, H8−H2′, and H8−H3′ is ca. 1:10:1.5, respectively (Figure S5B). There is no H8−H4′ NOE cross-peak. The strong NOE for H8−H2′, and the absence of an NOE between H8 and H4′, suggest a C2′-endo (*S*) anti conformation for the sugar ring. The value of ^3J (H1′/H2′) = 5.78 Hz for **8** is similar to that for free 5′-GMP (6.10 Hz). These data suggest that the C2′-endo anti-glycosidic sugar conformation of 5′-GMP is not altered by N7-binding to Ru.

NMR Structures of THA and DHA Complexes in Solution. [(η^6-$C_{14}H_{14}$)Ru(en)Cl]$^+$ (2) and [(η^6-$C_{14}H_{12}$)Ru(en)Cl]$^+$ (3) in DMSO-d_6. The 2D NOESY ^{1}H NMR spectrum of **2** in DMSO-d_6 provided a basis for the assignment of ^{1}H NMR resonances of **2** (Figure S7). There are strong NOEs between NH(u1, u2) and NH(d1, d2), between NH(u1, u2) and H(1, 4)/H(2, 3), between H(1, 4) and H(8, 9), and between H(8, 9) and H(5, 8). No NOEs were observed between NH(d1, d2) and aromatic protons. For **3**, the resonances were assignable directly from the 1D ^{1}H NMR spectrum (Figure S10). In each case, one set of sharp signals was observed for the THA/DHA ring.

[(η^6-$C_{14}H_{14}$)Ru(en)(9EtG-*N7*)]$^{2+}$ (6 and ^{15}N-6) and [(η^6-$C_{14}H_{14}$)Ru(en)(5′-GMP-*N7*)] (9 and ^{15}N-9) in Aqueous Solution. In contrast to the ^{1}H NMR resonances for the biphenyl complexes **4**, **5**, and **8**, the resonances of the tetrahydroanthracene rings of complexes **6** and **9** in aqueous solution were very broad, as were their G base and en ligand ^{1}H NMR resonances (Figures S8 and S9). When solutions of **6** and **9** were heated to 339 and 318 K, respectively, the peaks became sharper, but the resolution was not sufficient for NOESY studies. On cooling to 278 K, more than two sets of signals were detected in both cases, but chemical exchange processes complicated the interpretation of the NOESY data. 2D [^{1}H,^{15}N] HSQC NMR spectra of complexes **^{15}N-6** and **^{15}N-9** in aqueous solutions were acquired to confirm the assignment of the en NH signals, and the low-temperature spectra suggested the existence of two isomers (Table S7).

[(η^6-$C_{14}H_{12}$)Ru(en)(9EtG-*N7*)]$^{2+}$ (7) and [(η^6-$C_{14}H_{12}$)Ru(en)(5′-GMP-*N7*)] (10) in Aqueous Solution. The ^{1}H NMR resonances of the dihydroanthracene complexes **7** and **10** were very broad at ambient temperature. For complex **10**, two H8 signals were observed at 298 K (Figures S10 and S11). When the solutions of complexes **7** and **10** were heated to 339 and 318 K, respectively, the signals became sharper, but the resolution was not sufficient for 2D NOESY studies. At 278 K, more than two sets of signals were detected in both cases, but NOESY experiments at low temperatures were not attempted.

pH Dependence of NH Resonances of [(η^6-biphenyl)Ru(en)(5′-GMP-*N7*)] (8). We used ^{15}N-edited ^{1}H{^{15}N} NMR and pH titration methods to investigate H-bonding interactions between en NH and the 5′-phosphate or O6 groups of 5′-GMP in **^{15}N-8**. The 2D [^{1}H,^{15}N] HSQC NMR spectrum of **^{15}N-8** at 298 K showed four cross-peaks at δ 6.36/−29.04, 5.27/−29.04, 6.39/−29.01, and 5.09/−29.01, assignable to NH(u1), NH(d1), NH(u2), and NH(d2) (Figure 12A). 2D [^{1}H,^{15}N] HSQC NMR spectra of **^{15}N-8** were recorded over the pH range 2.8−10.9 and enabled the two NH(u) resonances to be distinguished on

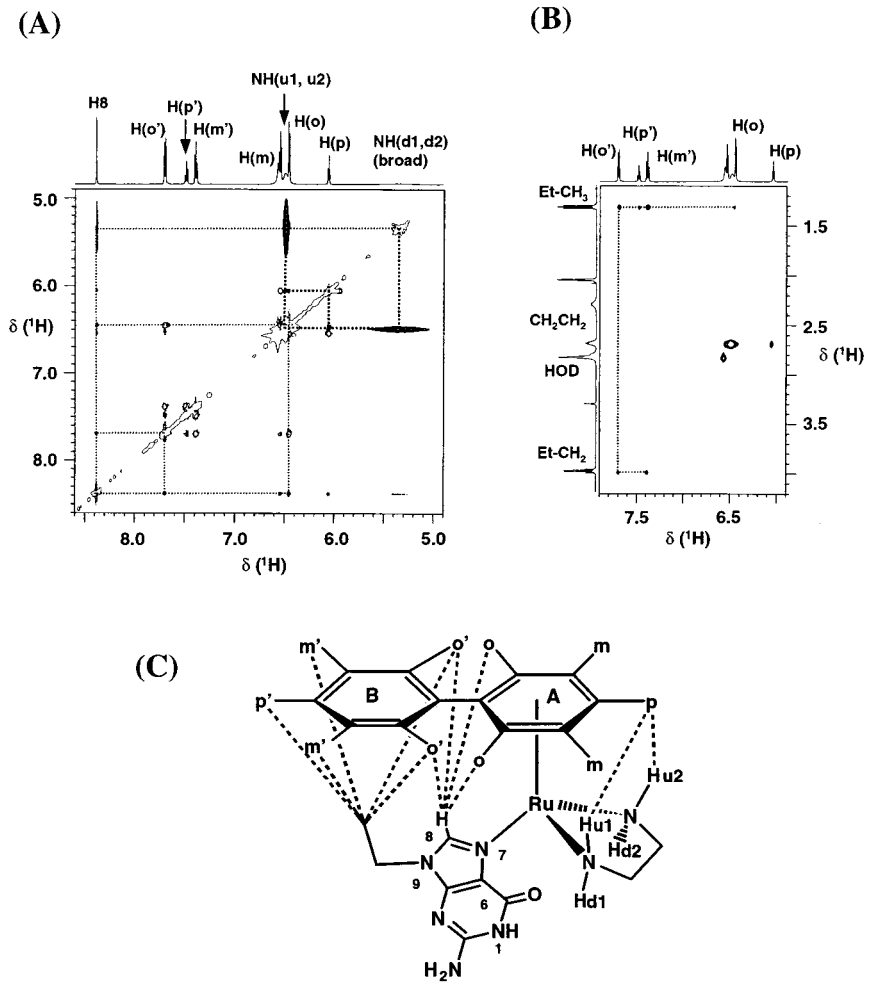

Figure 9. NOE data for [(η^6-biphenyl)Ru(en)(9EtG-*N7*)]$^{2+}$ (**4**). (A) and (B) Regions of the 2D NOESY ^{1}H NMR spectrum in acetone-d_6 at 298 K. (C) Structure with NOEs indicated by dotted lines. The en NH resonances were assigned via the [^{1}H,^{15}N] HSQC spectrum of **^{15}N-4** in acetone-d_6.

the basis of small differences in their ^{15}N chemical shifts. A plot of chemical shift of each en NH signal versus pH is shown in Figure 12D. The two NH(u1, u2) protons have the same pH dependence and shift slightly to high-field as the pH is increased; the two NH(d1, d2) protons also show similar pH behaviors and shift greatly to low-field over the range from pH 5.98 to 7.53. However, at pH < 5.98 or pH > 7.53 these two NH(d) peaks became too broad to observe.

^{1}H NMR and ^{31}P NMR pH titrations at 298 K were also carried out for a solution of unlabeled [(η^6-biphenyl)Ru(en)(5′-GMP-*N7*)] (**8**), containing a 10% excess of 5′-GMP. At pH 7.1, ^{1}H NMR peaks at δ 8.71 and δ 8.20 were observed for H8 protons of **8** and free 5′-GMP, respectively; ^{31}P NMR peaks at δ 4.61 and δ 3.96 were observed for the 5′-phosphate of **8** and free 5′-GMP, respectively. Plots of δ (^{1}H) and δ (^{31}P) against pH are shown in Figure 13. The curves were fitted to the Henderson−Hasselbalch equation, giving pK_a values of 5.96 for **8** and 6.30 for free 5′-GMP (^{1}H curves). These values are attributed to deprotonation of the 5′-phosphate groups. The pK_a values determined from the ^{31}P curves (Figure 13B, 5.93 and 6.24) are in good agreement with the values from ^{1}H curves. Also, pK_a values of 8.45 for complex **8** and 9.85 for free 5′-GMP were determined from the ^{1}H curves. These values are attributed to deprotonation of G N1H.

Discussion

There are many potential applications of organometallic chemistry in medicine. Examples include the anticancer activity of cyclopentadienyl complexes such as titanocence dichloride,[45] which is on clinical trial, and receptor-targeted anti-estrogen organometallic complexes.[46,47] Our current work is concerned with organometallic Ru(II) complexes of the type [(η^6-arene)-Ru(II)(en)Cl][PF_6] which exhibit promising anticancer activity. Initial in vitro and in vivo data suggest that the most active complexes contain the most hydrophobic η^6-arene ligands, examples being complexes **2** and **3** which contain the tricyclic η^6-anthracene derivatives THA and DHA.[6−8] In general, (η^6-arene)Ru(II) bonds are relatively stable in water[48] and are more resistant to hydrolysis than the Cp ligands in titanocene

(45) Köpf-Maier, P.; Köpf, H. In *Metal Compounds in Cancer Therapy*; Fricker, S. P., Ed.; Chapman & Hall: London, England, 1994; pp 109−146.
(46) Jaouen, G.; Top, S.; Vessieres, A.; Pigeon, P.; LeClercq, G.; Laios, I. *Chem. Commun.* **2001**, 383−384.
(47) Top, S.; Elhafa, M.; Vessieres, A.; Quivy, J.; Vaissermann, J.; Hughes, D. W.; McGlinchey, M. J.; Mornon, J. P.; Thoreau, E.; Jaouen, G. *J. Am. Chem. Soc.* **1995**, *117*, 8372−8380.
(48) (a) {(η^6-benzene)Ru(II)}$^{2+}$ exhibits high hydrolytic stability in water: Hung, Y.; Kung, W.-J.; Taube, H. *Inorg. Chem.* **1981**, *20*, 457−463. (b) Aqueous solutions of complexes **1**, **2**, and **3** show little evidence of arene dissociation even after 1 week at ambient temperature. We have chromatographed short single-stranded oligos containing one and two monofunctional N7-bound Ru adducts and isolated the fractions for MS or NMR and found that arene rings are still coordinated to Ru(II).

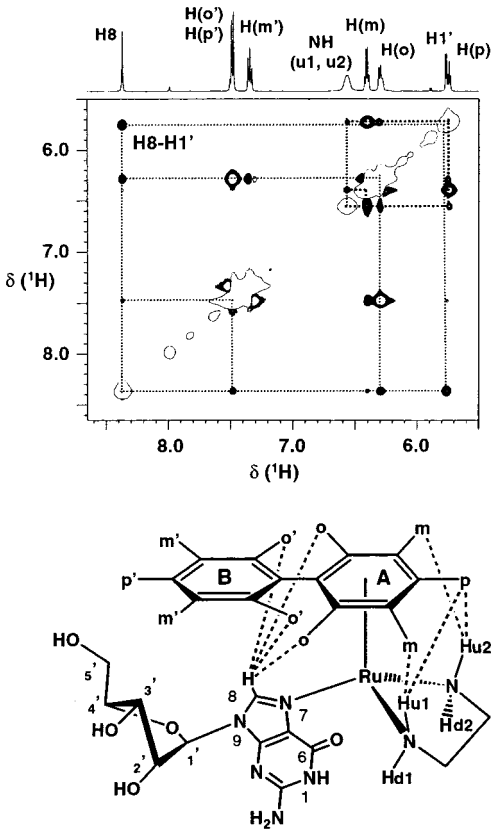

Figure 10. NOE data for [(η^6-biphenyl)Ru(en)(Guo-*N7*)]$^{2+}$ (**5**). Top: 2D NOESY ^{1}H NMR spectrum for **5** in 10% D_2O/90% H_2O at 298 K. Bottom: Structure with NOEs indicated by dotted lines.

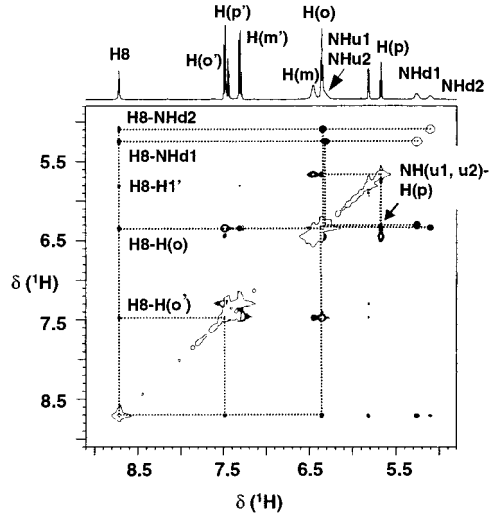

Figure 11. 2D NOESY^{1}H NMR spectrum of [(η^6-biphenyl)Ru(en)(5′-GMP-*N7*)] (**8**) in 10% D_2O/90% H_2O at 310 K, showing NOEs for H8−H(o′), H8−H(o), and H(p)−NH(u1,u2). The labeling scheme for **8** is similar to that for **5** in Figure 10.

dichloride, [Cp_2TiCl_2].[49] The target for Ru(II) arene complexes may be DNA, and we found that {(η^6-arene)Ru(II)(en)}$^{2+}$ exhibits a high specificity for binding to guanine (G).[7] The aim of the present work is to elucidate the nature of the interactions which gives rise to such specificity. We have therefore studied the structures and dynamics of adducts of {(η^6-arene)-Ru(II)(en)}$^{2+}$ with G derivatives both in the solid state and in solution.

Very few X-ray structures of Ru-nucleobase adducts have been reported previously.[50] The structure of [(η^6-biphenyl)-Ru(II)(en)(Guo-*N7*)][PF_6]$_2$·3.75(H_2O) determined in the present work appears to be the first reported X-ray structure for a ruthenium nucleoside complex. Also, no X-ray structures of η^6-coordinated DHA complexes appear to have been reported previously. We show that hydrophobic interactions of the arene ligand and H-bonds involving en NH protons exert a strong influence on the conformations of these guanine adducts.

Arene-Guanine Base Stacking. Strong arene-nucleobase stacking is present in the crystal structures of [(η^6-$C_{14}H_{14}$)Ru-(en)(9EtG-*N7*)]$^{2+}$ (**6**) and [(η^6-$C_{14}H_{12}$)Ru(en)(9EtG-*N7*)]$^{2+}$ (**7**). Figure 4A and B shows that $\pi-\pi$ stacking between the outer ring (C) of THA or DHA and the guanine base is almost ideal:[51] ring C is parallel to and fully overlaps the purine ring (see also Figure 7C and D). The THA ligand in complex **6** has a diene ring C, but it adopts a very similar conformation to the DHA ligand in complex **7** which contains an aromatic ring C. The interplanar (centroid−centroid) distance is 3.45 Å for complex **6** and 3.31 Å for **7**, with dihedral angles of 3.3° and 3.1°, respectively. The π-stacking of aromatic rings and unsaturated groups, or even between unsaturated groups themselves, has been widely investigated in studies of crystal engineering and energy transfer. Diene stacking has been employed in the design and control of polymer-chain structures.[52] For the biphenyl adduct **4**, [(η^6-biphenyl)Ru(en)(9EtG-*N7*)][PF_6]$_2$·MeOH, intramolecular arene-nucleobase stacking is precluded by the anti orientation of 9EtG with respect to biphenyl. Here, there is intermolecular stacking between the pendant phenyl ring and the purine six-membered ring (Figures 1B and S1A) with a centroid−centroid distance of 4.0 Å and dihedral angle of 4.5°. Such intermolecular arene-nucleobase stacking may stabilize the cyclic tetramer structure in the unit cell (Figure 1B). For adduct **5**, [(η^6-biphenyl)Ru(en)(Guo-*N7*)][PF_6]$_2$·3.75(H_2O), there are two types of stacking: intramolecular stacking of the pendant phenyl ring with the purine five-membered ring (3.8 Å, 23.8°), and intermolecular stacking of the purine six-membered ring with an adjacent pendant phenyl ring (4.2 Å, 23.0°). These occur alternately giving a columnar-type structure (Figure S1B). For aromatic systems, $\pi-\pi$ interactions are usually accompanied by interplanar separations of 3.3−3.8 Å.[51] However, longer distances for $\pi-\pi$ stacking have been also reported (up to 4.7 Å).[52a,c,53] The arene-nucleobase stacking in the biphenyl adducts **4** and **5** is accompanied by longer centroid−centroid distances (average 4.0 Å), as compared with that of THA and DHA adducts **6** and **7** (average 3.4 Å). This

(49) Toney, J. H.; Marks, T. J. *J. Am. Chem. Soc.* **1985**, *107*, 947−953.

(50) (a) [*cis*-Ru(II)(bpy)$_2$(9EtG)Cl]Cl·1.5H_2O: van Vliet, P. M.; Haasnoot, J. G.; Reedijk, J. *Inorg. Chem.* **1994**, *33*, 1934−1939. (b) [(η^6-C_6H_6)Ru(II)-(9EtG)$_2$(H_2O)][CF_3SO_3]$_2$: ref 9.

(51) Janiak, C. *J. Chem. Soc., Dalton Trans.* **2000**, 3885−3896. Of the various possible modes for π stacking of aromatic rings, face-to-face $\pi-\pi$ stacking appears to be optimized when both partners are electron-poor. The polarization of the arene and G ligands by Ru(II) may be an important factor for stabilization of arene-nucleobase stacking in the Ru(arene)-G complexes studied here.

(52) (a) Sarma, J. A. R. P.; Desiraju, G. R. *J. Chem. Soc., Perkin Trans. 2* **1985**, 1905−1912. (b) Merz, K. M.; Hoffmann, R.; Balaban, A. T. *J. Am. Chem. Soc.* **1987**, *109*, 6742−6751. (c) Matsumoto, A.; Odani, T.; Chikada, M.; Sada, K.; Miyata, M. *J. Am. Chem. Soc.* **1999**, *121*, 11122−11129.

(53) (a) Dietz, K.; Keller, H. J.; Nöthe, D.; Wehe, D. *J. Am. Chem. Soc.* **1982**, *104*, 7581−7585. (b) Vogt, T.; Faulmann, C.; Soules, R.; Lecante, P.; Mosset, A.; Castan, P.; Cassoux, P.; Galy, J. *J. Am. Chem. Soc.* **1988**, *110*, 1833−1840. (c) Hunter, C. A.; Sanders, J. K. M. *J. Am. Chem. Soc.* **1990**, *112*, 5525−5534.

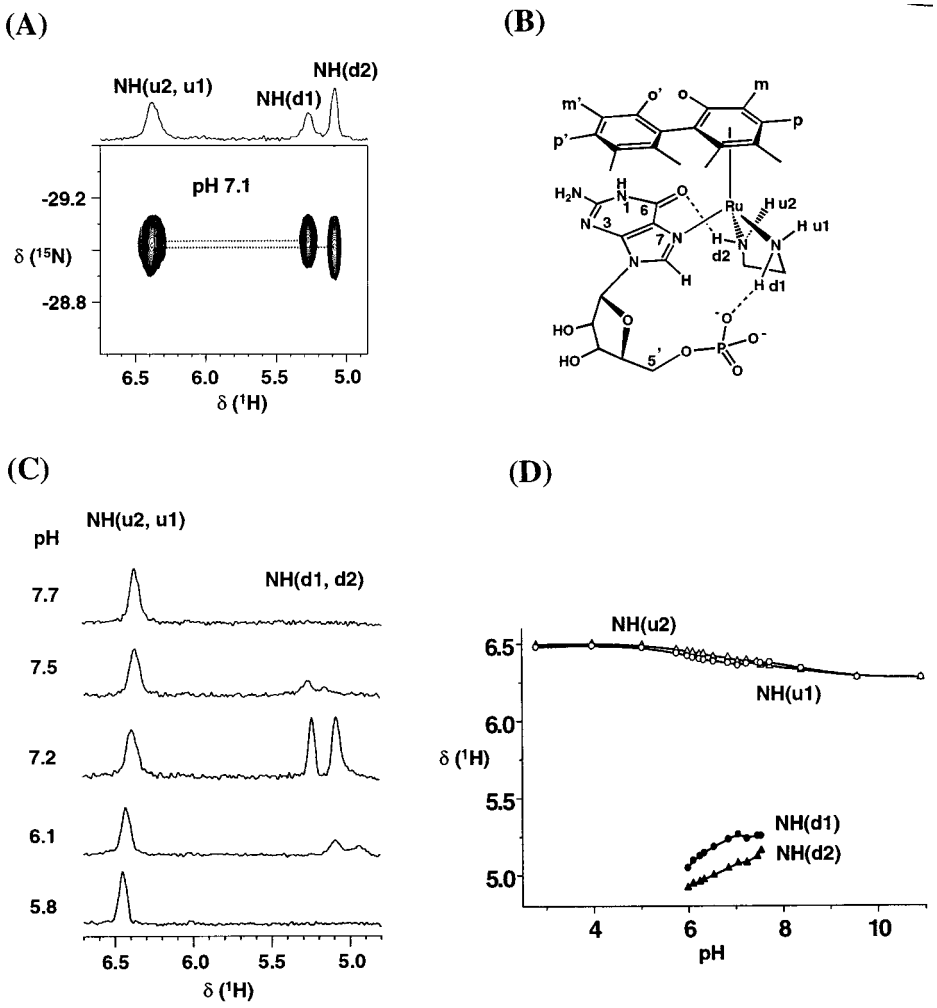

Figure 12. (A) 2D [^{1}H,^{15}N] HSQC NMR spectrum of [(η^6-biphenyl)Ru(^{15}N-en)(5′-GMP-*N7*)] (**^{15}N-8**) at pH 7.1 (Ru 5 mM, 10% D_2O/90% H_2O, 298 K). (B) Structure with proposed H-bonds indicated by dotted lines. (C) ^{15}N-edited ^{1}H{^{15}N} spectra at various pH values. (D) Plot of the chemical shifts of en $^{15}NH_2$ ^{1}H NMR resonances of **^{15}N-8** versus pH. The large variation in shift of the NH(d1, d2) protons can be accounted for by H-bonding interactions with the 5′-phosphate and G O6 groups, promoted by deprotonation of $-OPO_3H$ and N1H, respectively. The NH(d) resonances were too broad to observe both at high pH and at low pH.

can be accounted for by the higher degree of freedom[53c] for movement of the biphenyl ring (free propeller twisting of phenyl ring in Bip, but relatively rigid tricyclic frames of THA and DHA).

The extensive arene-nucleobase stacking but not arene-arene or base-base stacking in [(η^6-arene)Ru(en)(G-*N7*)]$^{2+}$ adducts represents a new structural feature for adducts of metal anticancer complexes with nucleobases. Intra- or intermolecular base-base stacking has been reported in the X-ray structures of some Pt complexes of nucleobases, nucleosides, and nucleotides. For example, *cis*-[(tn)Pt(Me-5′-GMP)$_2$], *cis*-[(tn)Pt(5′-IMP)$_2$] (tn = trimethylenediamine), and *cis*-[$(NH_3)_2$Pt(5′-IMP)$_2$] all have intracomplex base-base stacking with dihedral angles of 39.6°, 38.2°, and 40.7°, respectively.[54] Such features are relevant to the intrastrand cross-linking by *cis*-platinium complexes on DNA.[55] In the adducts of *cis*-[Pt(NH_3)(Guo)$_2$]$Cl_{1.5}(ClO_4)_{0.5}$·$7H_2O$ and *cis*-[Pt(en)(Guo)$_2$]$Cl_{1.5}I_{0.5}$·$2H_2O$, one guanine base is in nearly parallel contact with a guanine base on a neighboring cation at distances of 3.34 and 3.31 Å, respectively.[56] Stacking of acridine orange (AO) rings at a distance of 3.5 Å was found in the complex [Pt{AO$(CH_2)_6$(en)}(ox)](NO_3)·$7H_2O$, and the phi ligands of [Rh$(NH_3)_4$(phi)]$^{3+}$ (phi = 9,10-phenanthrenequinone diimine) cations stack in dimer pairs at a distance of 3.4 Å. This kind of self-stacking of aromatic rings has been interpreted as an indication of an ability to intercalate.[12,57] The arene-base stacking in [(η^6-arene)Ru(en)(G-*N7*)]$^{2+}$ adducts indicates potential for intercalation or hydrophobic interactions of the arene ring with duplex DNA. Hydrophobic interactions between the arene ligand and purine base could provide a driving force for DNA binding. A recent analysis of free energy contributions to DNA binding suggests that intercalation of ethidium, propidium, daunorubicin, and adriamycin is driven by hydrophobic effects and van der Waals contacts within the intercalation site, minimizing the solvent-accessible surfaces of the drug.[10] Recognition of specific sequences by DNA minor

(54) (a) Marzilli, L. G.; Chalilpoyil, P.; Chiang, C. C.; Kistenmacher, T. J. *J. Am. Chem. Soc.* **1980**, *102*, 2480−2482. (b) Marzilli, L. G. *Biochem. Biophys. Res. Commun.* **1978**, *84*, 70−75. (c) Kistenmacher, T. J.; Chiang, C. C.; Chalilpoyil, P.; Marzilli, L. G. *J. Am. Chem. Soc.* **1979**, *101*, 1143−1148.
(55) Marzilli, L. G. *Adv. Inorg. Biochem.* **1981**, *3*, 47−85.
(56) (a) Cramer, R. E.; Dahlstrom, P. L.; Seu, M. J. T.; Norton, T.; Kashiwagi, M. *Inorg. Chem.* **1980**, *19*, 148−154. (b) Gellert, R. W.; Bau, R. *J. Am. Chem. Soc.* **1975**, *97*, 7379−7380.
(57) Krotz, A. H.; Kuo, L. Y.; Barton, J. K. *Inorg. Chem.* **1993**, *32*, 5963−5974.

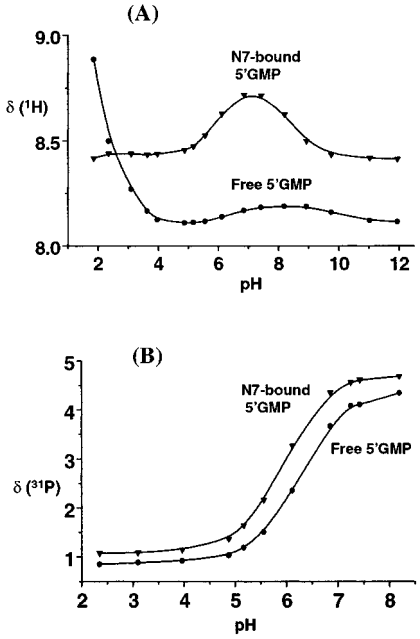

Figure 13. pH dependences of the 5′-GMP H8 ^{1}H (A) and phosphate ^{31}P (B) NMR resonances for [(η^6-biphenyl)Ru(en)(5′-GMP-*N7*)], **8** (▼) and free 5′-GMP (●) at 298 K, showing the lack of protonation of N7 for **8** at low pH, and deprotonation of N1 and phosphate at higher pH. The pK_a values for protonation of the phosphate group were determined to be 5.96 (^{1}H), 5.93 (^{31}P) for **8** and 6.30 (^{1}H), 6.24 (^{31}P) for free 5′-GMP, and for deprotonation of N1 of G, 8.45 (^{1}H) for **8** and 9.85 (^{1}H) for free 5′-GMP.

groove binding proteins is often dominated by hydrophobic protein−DNA interactions.[58] The X-ray crystal structure of HMG1 domain A bound to a cisplatin-modified 16-base-pair deoxyoligonucleotide shows that the cisplatin intrastand cross-link destacks the G_8-G_9 purine rings and leads to exposure of their hydrophobic surfaces in the minor groove. Phe37 intercalates at the site of the intrastand cross-link *cis*-[Pt(NH_3)$_2$-{d(GpG)-*N7*(G_8),-*N7*(G_9)}], stacking onto the G_9 base at a distance of 3.5 Å.[59] Favorable intercalation directs protein binding and orientation.[21]

Arene Conformation. The conformations of the parent chloro-complexes [(η^6-arene)Ru(en)Cl]$^+$ and guanine adducts [(η^6-arene)Ru(en)(G-*N7*)]$^{2+}$ are compared in Figure 6. In each case, there is a significant reorientation and conformational change of the arene ring with respect to the parent chloro-complex, as a result of arene−nucleobase interaction. For the biphenyl-guanine adducts **4** and **5**, the biphenyl ligand is rotated away from the Ru−N7 vector (around the arene-Ru π-bond) by 109.2° for **4**, and rotated back by 13.6° for **5**, as compared to the parent chloro-complex **1**, and is involved in inter- or intramolecular stacking with the purine ring (Table 4A). A decrease of ca. 10° in propeller twist of biphenyl for **4** and **5** (as compared to **1**) may also be driven by the phenyl-purine stacking force since there is no stacking interaction in **1**.

Arene-nucleobase stacking forces in **6** and **7** appear to cause large changes in the conformations of the THA and DHA ligands as compared with their parent chloro-complexes **2** and **3**, respectively (Figure 6C and D). When the Cl ligand in complex **2** is substituted by N7-G (complex **6**), the THA ligand rotates back around the arene-Ru π-bond by 19.5° (Table 4B**)** and relocates to a position where ring C is completely overlapped with the G base. Moreover, the planarity of this tricyclic frame is lost, and ring C bends down toward the purine about the C7A−C10A hinge by 27.8° (Table 4B). Similarly, the DHA ligand is rotated away from the Ru−Cl vector by 64.1° in **3**, and rotated back around the arene-Ru π-bond by 43.2° in **7** as compared to **3**, while ring C is bent down toward the Cl ligand about the C7A−C10A hinge by 40.6° in **3** and toward the purine by 31.9° in **7**. The increase of 35.3° in hinge bending angle for **6** and decrease of 8.7° for **7** as compared with their parent complexes **2** and **3**, respectively, allow ring C to make parallel contact with the purine in either case. Thus π-stacking interactions between the arene ring and nucleobase lead to arene ring reorientation and conformational adjustment.

The arene ligands possess flexibility through rotation around the arene-Ru π-bonds, propeller twisting for Bip, and hinge-bending for THA and DHA. These allow optimization of the geometry for simultaneous arene-base stacking with N7-covalent binding. When the Ru(arene) complex approaches DNA, the arene ligand could therefore adjust its conformation to accommodate interactions with the guanine base. This property may reduce the steric demands of the Ru drug and enhance DNA affinity. The steric requirement of the metal complex itself directly influences the rate of DNA binding and hence affects anticancer activity. The coordination of octahedral ruthenium complexes to DNA is more sterically demanding than for square-planar four-coordinated platinum complexes.[57,60] The antitumor complex *mer*-[Ru(III)(terpy)Cl_3] (terpy = 2,2′:6′,2″-terpyridine) can bind two guanine bases, and the rate of binding to calf thymus DNA is faster than that of the inactive complex *cis*-[Ru(II)(bpy)$_2Cl_2$] (bpy = 2,2′-bipyridine) which has one more rigid heterocyclic ring and binds to only one guanine base.[3c,50a,61] The binding of DNA bases to α-[Ru(II)(azpy)$_2Cl_2$] (azpy = 2-(phenylazo)pyridine) is sterically less-hindered than for *cis*-[Ru(II)(bpy)$_2Cl_2$]. The azpy ligand has flexibility since one ring is free from coordination to Ru, as compared with the rigid coordinated bpy ligand. α-[Ru(II)(azpy)$_2Cl_2$] has a very high cytotoxicity.[3d,62] The higher DNA reactivity of Na[*trans*-Ru(III)(Im)(DMSO)Cl_4] as compared to Na[*trans*-Ru(III)(Im)$_2$-Cl_4] (Im = imidazole) may also be related to the presence of two bulky heterocyclic axial ligands in the latter.[63]

Comparison between the crystal structures of complexes **4** and **5** suggests that the biphenyl ligand can adopt anti or syn conformations with respect to the G base (Figure 7A and B). In the crystal structures of **6** and **7**, the THA and DHA ligands both adopt a syn orientation (Figure 7C and D). In general, the orientation of arene ligand in G adducts may be different in the solid state as compared to in solution since both crystal packing and solvent effects can play a role. We studied the solution structures of guanine adducts using 2D NOESY NMR experiments in water or in acetone (dependent on solubility). The NOEs for its biphenyl adducts **4**, **5**, and **8** reveal that a syn

(58) (a) Jou, Z. S.; Chiu, T. K.; Leiberman, P. M.; Baikalov, I.; Berk, A. J.; Dickerson, R. E. *J. Mol. Biol.* **1996**, *261*, 239−254. (b) Grove, A.; Galeone, A.; Yu, E.; Mayol, L.; Geiduschek, E. P. *J. Mol. Biol.* **1998**, *282*, 731−739.
(59) Ohndorf, U. M.; Rould, M. A.; He, Q.; Pabo, C. O.; Lippard, S. J. *Nature* **1999**, *399*, 708−712.
(60) Sherman, S. E.; Gibson, D.; Wang, A. H.-J.; Lippard, S. J. *J. Am. Chem. Soc.* **1988**, *110*, 7368−7381.
(61) van Vliet, P. M.; Toekimin, S. M. S.; Haasnoot, J. G.; Reedijk, J.; Nováková, O.; Vrána, O.; Brabec, V. *Inorg. Chim. Acta* **1995**, *231*, 57−64.
(62) Hotze, A. C. G.; Velders, A. H.; Ugozzoli, F.; Biagini-Cingi, M.; Manotti-Lanfredi, A. M.; Haasnoot, J. G.; Reedijk, J. *Inorg. Chem.* **2000**, *39*, 3838−3844.
(63) Malina, J.; Nováková, O.; Keppler, B. K.; Alessio, E.; Brabec, V. *J. Biol. Inorg. Chem.* **2001**, *6*, 435−445.

orientation of the biphenyl ligand with respect to the G base predominates in solution in each case (Figures 9, 10, and 11). Accordingly, downfield shifts for resonances of the pendant phenyl ring protons (H(p′), H(o′), and H(m′)) in these three G adducts relative to those of the aqua biphenyl complex **1a** are observed. This effect is most pronounced for H(o′): $\Delta\delta$ = −0.36 (**4**), −0.33 (**5**), −0.34 (**8**) ppm (Table S4). Taken together, the syn orientation appears to be favored for [(η^6-biphenyl)Ru(en)(G-*N7*)] adducts both in the solid state and in solution. This can be attributed to hydrophobic interactions between the phenyl ring and purine base.

Fluxional Behavior of Arene Adducts. Structural studies on THA and DHA adducts in solution were also attempted. As compared with those of the parent chloro-complexes **2** and **3**, the ^{1}H NMR resonances of the THA and DHA rings in the guanine adducts **6**, **7**, **9**, **10** are broadened (Figures S8−S11). This may be due to the restricted rotation of the THA and DHA ligands. 2D [^{1}H,^{15}N] HSQC NMR spectra of **^{15}N-6** (274 K) and **^{15}N-9** (278 K) in water both show two sets of NH cross-peaks attributable to the presence of two isomers A and B (probably corresponding to anti and syn conformations) (Table S7). The 2D NMR EXSY-NOESY spectra (278 K) of **^{15}N-9** (not shown) indicated exchange among two possible conformations at low temperature. The fluxionality of organometallic complexes has been previously investigated.[64] Very small rotational barriers have been calculated for (η^6-benzene)Ru(II) complexes, and restricted rotation about the Ru-arene π-bond has been observed only on the presence of particular electronic and steric factors.[65] For biphenyl adducts, there is no obvious broadening of the biphenyl ring resonances for complexes **4**, **5**, and **8** at various temperaures (273−318 K), indicating free rotation of the biphenyl ligand. However, the resonances for Guo and 5′-GMP in **5** and **8** do broaden at low temperature. In the case of **^{15}N-8**, two sets of en NH [^{1}H,^{15}N] cross-peaks were present at 274 K (Figure S6B), and the H8 ^{1}H signal separated into two. This can be attributed to slow rotation of G at low temperature. Thus it appears that G rotation is more restricted than biphenyl rotation. This is not surprising since the G base forms one leg of the "piano-stool", and its movement is restricted by both the arene and the en ligands. Synchronous movements of the pendant phenyl ring and the G base may be possible with propeller twisting of the pendant phenyl ring. Such movement would not be possible for THA and DHA adducts which have relatively rigid tricyclic rings and explains why free rotation of the biphenyl rings is little affected by the steric factors from the G base in the biphenyl adducts in contrast to the THA and DHA adducts.

H-Bonding Interactions. The crystal structures of the guanine adducts **4**, **5**, **6**, and **7** show that en NH protons are involved in stereospecific H-bonding. The average N···O distance of 2.8 Å and N−H···O angle of 163° are indicative of the strong N−H···O hydrogen-bonding between one en NH(d) proton and the G O6 oxygen (Table 3). H-bonding interactions between the other en NH(d) proton and ribose O(5′) in the Guo adduct **5** are not present since the N···O distances, 3.7 Å in cation I and 5.3 Å in cation II, are long as in the reported Pt-Guo adducts.[66] The two NH(u) protons of en are not involved in the intramolecular H-bonding with G O6 but in relatively weak H-bonding with the counterion PF_6^- or with G O6 of a neighboring molecule. Such stereospecific H-bonding suggests that the en ligand may locate in a specific position to H-bond to the neighboring exocylic oxygen atoms of the bases (or a phosphate group) and thus influence the site recognition of {(η^6-arene)Ru(II)(en)}$^{2+}$ when covalently bound to DNA. The site-recognition ability of octahedral metallointercalators has been improved by the introduction of aliphatic ancillary ligands. For example, [Rh(NH$_3$)$_4$phi]$^{3+}$, [Rh(en)$_2$phi]$^{3+}$, and [Rh[12]aneN$_4$phi]$^{3+}$ (phi = 9,10-phenanthrenequinone diimine) bind to 5′-GC-3′ sites. This sequence specificity is related to H-bonding between the axial amines of these metal complexes and the O6 of G.[23] The crystal structure of Δ-α-[Rh[(R,R)Me$_2$trien]phi]$^{3+}$ bound to 5′-GTTGCAAC-3′ clearly shows sequence-specific interactions between the thymine methyl group and DNA, including H-bonding between axial amines and G O6 with an average N···O distance of 2.9 Å and H−N···O angle of 165°.[24] Platinum am(m)ine complexes also show H-bonding involving am(m)ine ligands in their nucleobase adducts in the solid state. For example, there is intermolecular H-bonding between the G O6 and the en NH of a neighboring molecule in [Pt(en)(Guo)$_2$]Cl$_{1.5}$·I$_{0.5}$·2H$_2$O,[56b] weak intramolecular H-bonding between an ammine NH and a G O6 in *cis*-[Pt(NH$_3$)$_2$\{d(CpGpG)-*N7*(2),*N7*(3)\}]$^{2+}$,[67] and weak intermolecular ammine-O6 H-bonding but stronger intramolecular H-bonding with the terminal 5′-phosphate in *cis*-[Pt(NH$_3$)$_2$\{d(pGpG)-*N7*(1),*N7*(2)\}]$^{2+}$.[60] Such H-bonding interactions of NH ligands are thought to play a major role in determining the nature of platinated DNA adducts,[26a] and this may be an important factor for the antitumor activity.[68] Similarly, en NH H-bonding may be important for the activity of Ru(II) arene complexes. Moreover, Ru−N bonds form the legs of the piano stool and impose much tighter steric constraints in comparison with planar Pt am(m)ine complexes. The NH(d) but not NH(u) protons are correctly oriented for intramolecular H-bonding with G O6. This strong intramolecular NH···O6 H-bonding may partly account for the high selectivity of {(η^6-arene)Ru(II)(en)}$^{2+}$ binding to guanine with little binding to adenine, cytosine, or thymine, when in competition. Although many reported Pt and Ru complexes also bind covalently to adenine derivatives,[1,26a] this does not appear to be the case for [(η^6-arene)Ru(en)Cl]$^+$.[7]

Guanine is involved in intermolecular N2H···N3 base pairing in the three 9EtG adducts **4** (Figure 1A), **6** (Figure S3), and **7** (Figure 5). Such dimerization has been observed in a number of Pt(II) crystal structures containing purine derivatives.[69] In the case of complex **5**, base pairing is not observed; instead, the NH2 of G participates in H-bonding with O(32) of the sugar from a neighboring cation, and with O(19)W of water (Table 3B). The overall structure of **5** contains a complicated H-bonding

(64) Muetterties, E. L.; Bleeke, J. R.; Wucherer, E. J. *Chem. Rev.* **1982**, *82*, 499−525 and references therein.
(65) (a) Albright, T. A.; Hoffmann, R.; Tse, Y.-C.; D'Ottavio, T. *J. Am. Chem. Soc.* **1979**, *101*, 3812−3821. (b) Pomeroy, R. K.; Harrison, D. J. *J. Chem. Soc., Chem. Commun.* **1980**, 661−663. (c) Chudek, J. A.; Hunter, G.; Mackay, R. L.; Kremminger, P.; Weissensteiner, W. *J. Chem. Soc., Dalton Trans.* **1991**, 3337−3347.
(66) (a) Bau, R.; Gellert, R. W.; Lehovec, S. M.; Louie, S. *J. Clin. Hematol. Oncol.* **1977**, *7*, 51−62. (b) Cramer, R. E.;. Dahlstrom, P. L. *J. Clin. Hematol. Oncol.* **1977**, *7*, 330−337. (c) Melanson, R.; Rochon, F. D. *Can. J. Chem.* **1978**, *57*, 57−61.
(67) Admiraal, G.; van der Veer, J. L.; de Graaff, R. A. G.; den Hartog, J. H. J.; Reedijk, J. *J. Am. Chem. Soc.* **1987**, *109*, 592−594.
(68) Cleare, M. J.; Hoeschele, J. D. *Bioinorg. Chem.* **1973**, *2*, 187−210.
(69) (a) Dieter-Wurm, I.; Sabat, M.; Lippert, B. *J. Am. Chem. Soc.* **1992**, *114*, 357−359. (b) Witkowshi, H.; Freisinger, E.; Lippert, B. *J. Chem. Soc., Chem. Commun.* **1997**, 1315−1316. (c) Sigel, R. K. O.; Freisinger, E.; Metzger, S.; Lippert, B. *J. Am. Chem. Soc.* **1998**, *120*, 12000−12007.

network involving the en group, purine, PF_6^- ion, and water molecules (nine per unit cell). Water is an important participant in intercalation complexes, and the specific binding of water to DNA complexes can make a significant contribution to the free energy of drug binding.[70] The presence of numerous water molecules together with PF_6^- ions contributes to the stabilization of the columnar-type stacking in [(η^6-biphenyl)Ru(en)(Guo-*N7*)]-$[PF_6]_2 \cdot 3.75H_2O$ (**5**). The 9EtG adducts **4**, **6**, and **7** also form interesting polymeric structures in the solid state. Figure 5 shows the right-handed helical chain-type structure of **7**, which displays G−G base pairing, intramolecular N−H···O6 H-bonds, intermolecular N−H···O6 H-bonds, and intramolecular stacking of ring C with the purine of 9EtG.

Attempts to prepare X-ray-quality single crystals of [(η^6-biphenyl)Ru(en)(5′-GMP-*N7*)] (**8**) were not successful, but NMR studies allowed investigation of NH H-bonding interactions in aqueous solution. ^{31}P and ^{15}N-edited ^{1}H NMR and 2D [^{1}H,^{15}N] NMR methods have been used previously to detect NH H-bonding to 5′-phosphate and G O6 groups in Pt-am(m)ine adducts of G derivatives.[26d,71−73] Similarly, we have used ^{15}N-edited ^{1}H{^{15}N} NMR and ^{31}P NMR spectroscopy together with pH titration methods to investigate the role of en NH protons in **^{15}N-8**.

With an increase in pH from 2.8 to 10.9, the two NH(u1, u2) protons of **^{15}N-8** exhibit a similar pattern of chemical shift changes, becoming slightly shielded, while the two NH(d1, d2) protons also exhibit the same behavior but become greatly deshielded (Figure 12). Similar data have been reported for [Pt-(^{15}N-en)(5′-AMP)$_2$]$^{2+}$, for which one en NH is capable of H-bonding with 5′-phosphate and becomes greatly deshielded, but the other proton on the same en N is incapable of H-bonding and becomes slightly shielded as the pH increases.[26d] The NH-(d1, d2) protons of **8** point toward 5′-GMP as shown in the solution structure of **8** (Figure 11) and are capable of H-bonding with the 5′-phosphate[74] and G O6. This H-bonding is promoted by deprotonation of the 5′-phosphate and N1H groups.[71b] The pK_a of the 5′-phosphate group of **8** is 5.93, 0.31 units lower than that of free 5′-GMP (6.24, Figure 13B), attributable to the increased stabilization of deprotonated phosphate via H-bonding. This can be compared to a lowering of the 5′-phosphate pK_a value for [Pt(en)(5′-GMP)$_2$]$^{2+}$ by 0.38 units,[26d] and for [Pt(en)-(5′-AMP)$_2$] by 0.4 units.[75] The pK_a of G N1H of **8** is 8.45, 1.28 units lower than that of free 5′-GMP (9.73[76]). For comparison, the pK_a of G N1H is lowered by ca. 0.9−1.3 when guanine derivatives are coordinated to Pt(II) via N7,[77] for example, 1.1 units for [Pt(dien)(5′-GMP)].[71b] Lowerings of 0.8 for [Ru(II)-$(NH_3)_5$(HGuo)]$^{2+}$ and of 2.2 for [Ru(III)$(NH_3)_5$(HGuo)]$^{3+}$ have been reported. The acidifying efffect of Ru(II) is therefore lower than that of Ru(III), attributable not only to the lower charge of Ru(II), but also to a smaller degree of back-donation of electron density.[2,78] The larger lowering of pK_a (1.28) in complex **8** may be associated partly with N7 coordination to Ru(II) and partly with strong (N1$^-$)−C═O (N1═C−O$^-$) H-bonding with en NH.[2]

At pH > 7.53, NH(d1) and NH(d2) resonances of **^{15}N-8** both became too broad to observe. This may be due to more restricted rotation of G about Ru−N7 due to the formation of stronger H-bonding at high pH or due to base-catalyzed proton exchange.[79] The effect of restricted rotation of G on the broadening of en NH(d1, d2) resonances was also observed for [(η^6-biphenyl)Ru(II)(^{15}N-en)(Guo-*N7*)]$^{2+}$ (**^{15}N-5**). The two NH(d) resonances disappeared when the temperature was below 328 K, but sharpened above 328 K due to faster G rotation (see Figure S6A and Table S7). The NH(d1, d2) signals of **^{15}N-8** also disappeared at pH < 5.96 (Figure 12), perhaps due to overlap with the water resonance. The en NH resonances of [Pt(^{15}N-en)(5′-GMP)$_2$] and [Pt(^{15}N$_2$-dien)(5′-GMP)] have been reported to disappear, but outside a much wider pH range (3−9.5).[26d,71b] The pH dependence of the chemical shift of NH-(u1, u2) of **^{15}N-8** shows little evidence of strong H-bonding with the 5′-phosphate or G O6 groups. This result is in accordance with the X-ray crystal structures of [(η^6-biphenyl)-Ru(en)(9EtG-*N7*)]$^{2+}$ (**4**) and [(η^6-biphenyl)Ru(en)(Guo-*N7*)]$^{2+}$ (**5**): NH(u1, u2) are on the opposite side to NH(d1, d2) and point away from 5′-GMP. The high stereospecificity leads to the formation of strong H-bonds.

Conclusions

We have designed organometallic Ru(II) complexes which incorporate several DNA recognition features. The Ru(II) center has a reactive coordination site and can form monofunctional adducts with DNA. The π-bonded arene ligand has potential to form hydrophobic and van der Waals contacts with nucleobases, and the diamine ligand has NH groups available for H-bonding.

We have shown that arene−nucleobase interactions and stereospecific H-bonding are present in [(η^6-arene)Ru(en)(G-*N7*)] adducts both in the solid and in solution. The presence of arene−nucleobase interactions suggests that the η^6-arene ligand could intercalate into DNA. The arene ligands especially possess conformational flexibility through rotation around the arene-Ru π-bonds, propeller twisting for biphenyl, and hinge bending for the anthracene derivatives THA and DHA. These make simultaneous arene-nucleobase stacking and N7-covalent binding compatible. The conformational flexibility can also reduce the steric requirements of the Ru drug and enhance DNA affinity. Stereospecific H-bonding to G O6 involves only en NH(d) protons (oriented away from the arene) and not NH(u) protons (oriented toward the arene) and partly accounts for the high preference of {(η^6-arene)Ru(en)}$^{2+}$ for binding to G versus A.

Our studies on these model compounds suggest a new potential DNA-binding mode for ruthenium anticancer drugs, involving simultaneous intercalation and covalent coordination with DNA. Such features may lead to highly specific recognition of

(70) Qu, X.; Chaires, J. B. *J. Am. Chem. Soc.* **2001**, *123*, 1−7.
(71) (a) Berners-Price, S. J.; Ranford, J. D.; Sadler, P. J. *Inorg. Chem.* **1994**, *33*, 5842−5846. (b) Guo, Z.; Sadler, P. J.; Zang, E. *J. Chem. Soc., Chem. Commun.* **1997**, 27−28.
(72) Xu, Y.; Natile, G.; Intini, F. P.; Marzilli, L. G. *J. Am. Chem. Soc.* **1990**, *112*, 8177−8179.
(73) (a) Fouts, C. S.; Marzilli, L. G.; Andrew Byrd, R.; Summers, M. F.; Zon, G.; Shinozuka, K. *Inorg. Chem.* **1988**, *27*, 366−376. (b) Bloemink, M. J.; Heetebrij, R. J.; Inagaki, K.; Kidani, Y.; Reedijk, J. *Inorg. Chem.* **1992**, *31*, 4656−4661.
(74) In the crystal structure of [(η^6-biphenyl)Ru(en)(Guo)][PF_6]$_2 \cdot 3.75H_2O$ (**5**), the distance between ribose O(5′) and NH(d) is long: 3.7 Å in cation I and 5.3 Å in cation II. If similar sugar conformations are adopted by [(η^6-biphenyl)Ru(en)(5′-GMP)] (**8**), then H-bonding of en N−H(d) protons with the 5′-phosphate of 5′-GMP is possible since the 5′-phosphate oxygen can closely approach the NH(d) protons.
(75) Reily, M. D.; Marzilli, L. G. *J. Am. Chem. Soc.* **1986**, *108*, 6785−6793.
(76) Scheller, K. H.; Scheller-Krattiger, V.; Bruce Martin, R. *J. Am. Chem. Soc.* **1981**, *103*, 6833−6839.
(77) (a) Inagaki, K.; Kidani, Y. *J. Inorg. Biochem.* **1979**, *11*, 39−47. (b) Schröder, G.; Lippert, B.; Sabat, M.; Lock, C. J. L.; Faggiani, R.; Song, B.; Sigel, H. *J. Chem. Soc., Dalton Trans.* **1995**, 3767−3775.
(78) Clarke, M. J.; Taube, H. *J. Am. Chem. Soc.* **1974**, *96*, 5413−5419.
(79) (a) Basolo, F.; Pearson, R. G. *Mechanisms of Inorganic Reactions*, 2nd ed.; Wiley: New York, 1967; pp 33, 184. (b) Lichtig, J.; Sosa, M. E.; Tobe, M. L. *J. Chem. Soc., Dalton Trans.* **1984**, 581−585.

bases in DNA duplexes and may be useful for optimizing the anticancer activity of organometallic Ru(II) arene anticancer complexes. Initial studies using CD, LD, and melting experiments[80] suggest that monofunctional binding of Ru(II) arene can cause significant perturbation to the structure of calf thymus DNA, accompanied by intercalation in some cases.

Acknowledgment. We thank the CVCP (ORS Award for H.C.), EPSRC, ETF, Wolfson Foundation, and Royal Society for their support for this work, and our colleagues in EC COST D8 and D20, and in the ICRF Oncology Unit, Western General Hospital (Edinburgh), for stimulating discussions. We also thank Dr. Robert Morris, Dr. Abraha Habtemariam, and Dr. Hye-seo Park (University of Edinburgh) for experimental assistance, and Dr. Juan Mareque (University of Edinburgh) for helpful discussions and for comments on this script.

(80) Chen, H.; Nováková, O.; Zaludová, R.; Brabec, V.; Sadler, P. J., unpublished results.

Supporting Information Available: Tables S1−S7 listing X-ray bond lengths and angles for complexes **1**−**7**, H-bonding interactions involving water and sugar oxygens in **5**, X-ray characterization data for the ribose conformations of **5**, ^{1}H NMR chemical shifts for complexes **1**, **1a**, **4**, **5**, and **8**, interligand NOEs for **1**, **4**, **5**, and **8**, ^{1}H and ^{15}N NMR chemical shifts for **^{15}N-4**, **^{15}N-5**, **^{15}N-6**, and **^{15}N-9** at various temperatures. Figures S1−S11 showing stacking in crystalline **4** and **5**, the H-bond network in crystals of **6**, 2D [^{1}H,^{1}H] COSY NMR spectrum of **1**, 2D [^{1}H,^{1}H] DQFCOSY NMR spectrum of **4**, 2D [^{1}H,^{1}H] NOESY NMR spectra of **2**, and of **5** and **8** (sugar region), 2D [^{1}H,^{15}N] HSQC NMR spectra of **^{15}N-5** and **^{15}N-8** at various temperatures, ^{1}H NMR spectra of **2** and **3**, temperature dependence of ^{1}H NMR spectra of **6**, **7**, **9**, and **10** (PDF). X-ray crystallographic data are also available in CIF format. This material is available free of charge via the Internet at http://pubs.acs.org.

JA017482E